







Allosteric links between the hydrophilic N-terminus and transmembrane core of human Na⁺/H⁺ antiporter NHA2

Diego Velázquez¹  | Vojtěch Průša¹ | Gal Masrati²  | Elon Yariv²  |
Hana Sychrova¹  | Nir Ben-Tal²  | Olga Zimmermannova¹ 

¹Laboratory of Membrane Transport, Institute of Physiology of the Czech Academy of Sciences, Prague, Czech Republic

²Department of Biochemistry and Molecular Biology, George S. Wise Faculty of Life Sciences, Tel-Aviv University, Tel-Aviv, Israel

Correspondence

Olga Zimmermannova, Institute of Physiology CAS, Laboratory of Membrane Transport, Videnska 1083, Prague 4—Krc, 142 20, Czech Republic.

Email: olga.zimmermannova@fgu.cas.cz

Funding information

Grantová Agentura České Republiky, Grant/Award Number: 21-08985S; IPHYS Mobility II, Grant/Award Number: CZ.02.2.69/0.0/0.0/18_053/0016977; USA-Israel Binational Science Foundation and the Abraham E. Kazan Chair in Structural Biology, Tel Aviv University, Grant/Award Number: 2017293

Review Editor: John Kuriyan

Abstract

The human Na⁺/H⁺ antiporter NHA2 (*SLC9B2*) transports Na⁺ or Li⁺ across the plasma membrane in exchange for protons, and is implicated in various pathologies. It is a 537 amino acids protein with an 82 residues long hydrophilic cytoplasmic N-terminus followed by a transmembrane part comprising 14 transmembrane helices. We optimized the functional expression of *HsNHA2* in the plasma membrane of a salt-sensitive *Saccharomyces cerevisiae* strain and characterized in vivo a set of mutated or truncated versions of *HsNHA2* in terms of their substrate specificity, transport activity, localization, and protein stability. We identified a highly conserved proline 246, located in the core of the protein, as being crucial for ion selectivity. The replacement of P246 with serine or threonine resulted in antiporters with altered substrate specificity that were not only highly active at acidic pH 4.0 (like the native antiporter), but also at neutral pH. P246T/S versions also exhibited increased resistance to the *HsNHA2*-specific inhibitor phloretin. We experimentally proved that a putative salt bridge between E215 and R432 is important for antiporter function, but also structural integrity. Truncations of the first 50–70 residues of the N-terminus doubled the transport activity of *HsNHA2*, while changes in the charge at positions E47, E56, K57, or K58 decreased the antiporter's transport activity. Thus, the hydrophilic N-terminal part of the protein appears to allosterically auto-inhibit cation transport of *HsNHA2*. Our data also show this in vivo approach to be useful for a rapid screening of SNP's effect on *HsNHA2* activity.

KEYWORDS

human NHA2, Na⁺/H⁺ antiporter, N-terminal auto-inhibition, phloretin, yeast

1 | INTRODUCTION

The maintenance of ion homeostasis is crucial for any living cell, as it influences various physiological parameters such as cell size, intracellular pH, and membrane potential. Cation/H⁺ antiporters (CPAs, SLC9 family) are tightly regulated transporters that ensure appropriate

intracellular concentrations of monovalent cations in organisms of all kingdoms, from bacteria to mammals.¹ They mediate the exchange of monovalent cations, mainly Na⁺ and K⁺, for one or two protons across the membrane. Human cation/H⁺ antiporters account for 13 isoforms from three subfamilies—NHE (SLC9A), which includes 9 proteins (NHE1-9), NHA (SLC9B) with

two members, NHA1 and NHA2, and the SLC9C subfamily with two proteins (SLC9C1 and SLC9C2) of unknown functions.^{2,3} Deficiencies in the functions of CPAs are related to a growing list of pathologies, ranging from hypertension to autism spectrum disorder and cancer, which demonstrates their importance for human health.³

In this work we focus on a member of the SLC9B subfamily encoded by the NHA2 gene. It is a $\text{Na}^+(\text{Li}^+)/\text{H}^+$ antiporter, which is expressed in multiple tissues,⁴ but its physiological functions are relatively poorly defined. Within individual cells, it was shown to be localized to the plasma membrane or intracellularly to endosomes or mitochondria.^{4,5} It generally contributes to the regulation of intracellular pH, sodium homeostasis, and cellular volume, and it was found to play crucial roles in various physiological processes depending on the specific tissue where it resides.

All knowledge obtained so far indicates that NHA2 performs multiple functions in the human body and its malfunctioning leads to various pathologies ranging from metabolic to fertility disorders. Moreover, the NHA2 gene is located in a human chromosomal region (4q24) which has been associated with hypertension in numerous linkage studies.⁶ So far, particular physiological roles of NHA2 have been studied in a range of organisms and tissues. Single RNAi knockdowns of NHA2 or its homolog NHA1 in *Drosophila melanogaster* reduced survival, and their combination was lethal, suggesting their essentiality for life.⁷ In pancreatic β -cells of mice and humans, NHA2 resides in endosomes and is critical for insulin secretion and clathrin-mediated endocytosis.⁸ The loss of NHA2 also exacerbates obesity- and aging-induced glucose intolerance in mice,⁹ and a single-nucleotide polymorphism of the NHA2 locus was recently associated with type 2 diabetes in humans.¹⁰ In the kidney, NHA2 localizes to distal convoluted tubules, where it is critical for electrolyte (sodium reabsorption) and blood pressure homeostasis.^{4,11} In 2021, Anderegg et al. corroborated the NHA2 role in blood pressure regulation in mice, and identified it as critical for the maintenance of serine–threonine with-no-lysine kinase 4 (WNK4) levels, and thus ultimately for the activity of the Na^+/Cl^- co-transporter NCC in the distal convoluted tubules of the kidney.¹² Increased NHA2 expression also promotes cyst development in an in vitro model of polycystic kidney disease.¹³ In the testis, NHA2 is relevant for sperm motility and male fertility, since the deletion of NHA2 significantly reduced the percentage of motile sperm (of about 30%) and resulted in a decrease in pregnancy rate (of about 25%) in mice.¹⁴ In addition, several studies showed NHA2 to be expressed in osteoclasts, where NHA2 depletion significantly inhibited osteoclast differentiation

in vitro^{5,15,16}; however, its physiological role in vivo in this type of cell remains to be elucidated.^{17,18}

As for its structure, human NHA2 is a protein 537 amino acids in length and 58 kDa in size. It consists of 14 transmembrane segments (TMS), a hydrophilic N-terminus approximately 82 amino acids long, and a relatively short (27 aa) hydrophilic C-terminus. A two-dimensional representation of *HsNHA2* topology is schematically shown in Figure 1a, and in detail in Figure S1. Recently, 3D-structures of human NHA2 and its bison homolog were determined using cryo-electron microscopy (Protein Data Bank 7B4M and 7B4L,²³ respectively). However, the hydrophilic N-terminal and C-terminal parts of NHA2 were not resolved in both structures. The N- and C-termini are predicted to be unstructured, for example by the recently published AI-based protein structure prediction algorithm AlphaFold2.²⁴ The importance of the highly unstructured hydrophilic N-terminal part for the functioning of NHA2 has not been studied yet. In general, methods such as x-ray crystallography and cryo-electron microscopy are limited when it comes to extremely mobile and unstructured regions of proteins. In the case of CPAs, many mammalian antiporters possess extramembrane regions mostly in their N- or C-termini, which are predicted to be unstructured. These are often involved in regulatory mechanisms and interaction with other proteins.^{25–28} Indeed, despite the growing number of CPAs structures our understanding of the function of these regulatory regions remains limited.

HsNHA2 mediates an electroneutral efflux of sodium or lithium cations in exchange for external protons across the membrane.^{7,29} Some studies indicate that, depending on the proton or cation concentrations, it is able to work in both directions and also provides Na^+/Li^+ counter transport in kidney-derived MDCK cells.^{11,30} Pharmacologically, NHA2 is resistant to amiloride, a typical inhibitor of members of the NHE subfamily, but it is a phloretin-sensitive transport system.^{6,30}

So far, several functional and mutagenesis studies of *HsNHA2* have been done upon its expression in the model yeast *S. cerevisiae*, in a strain that lacked the three Na^+ transporters—the Na^+/H^+ antiporter Nha1 and Na^+ -ATPases Ena from the plasma membrane and the endosomal Na^+/H^+ antiporter Nhx1.^{4,6,23,31} This strain is highly sensitive to all alkali-metal-cations salts and the expression of *HsNHA2* improved the growth of these cells in the presence of sodium or lithium in a pH dependent manner.^{4,6} Examination of the growth of yeast cells expressing mutated variants of *HsNHA2* in the presence of salts was also used to identify some residues that are important for the activity of *HsNHA2*.^{23,31} However, the transport activity of the native (or mutated) *HsNHA2*

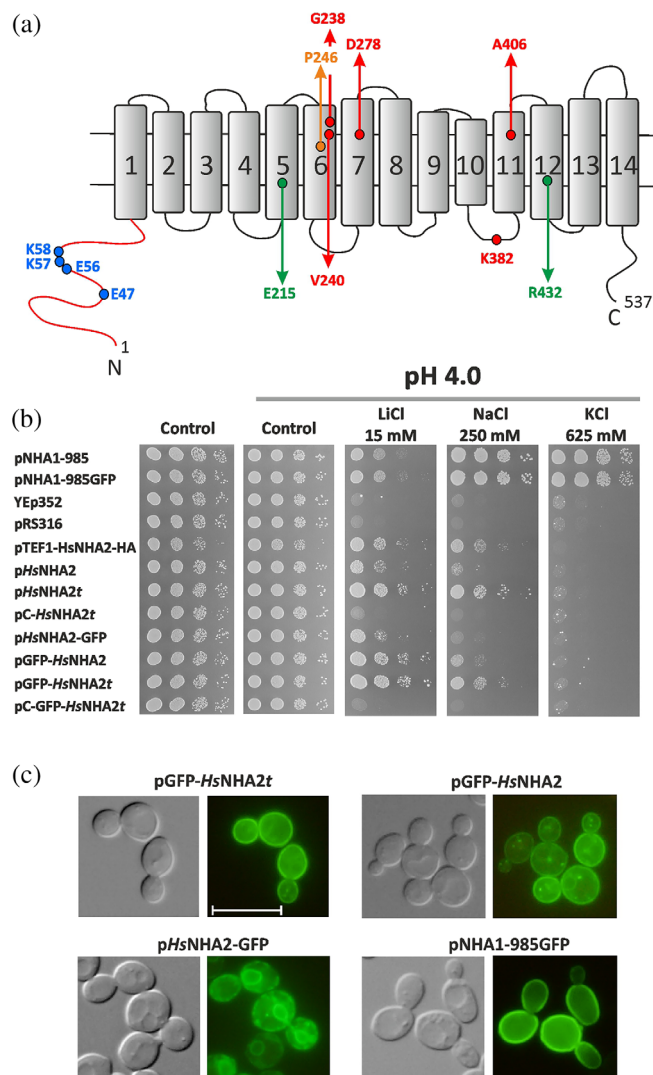


FIGURE 1 Optimization of conditions for heterologous expression of *HsNHA2* in *S. cerevisiae*. (a) Schematic representation of transmembrane topology of *HsNHA2*. The positions of residues studied in this work are highlighted. (b) Growth of alkali-metal cation-sensitive BW31 strain containing empty vectors (YEp352, pRS316) or expressing *ScNha1* or *HsNHA2* (non-tagged or N- or C-terminally tagged with GFP) from various types of plasmids (Table 1) was compared on YNB-Pro (pH approx. 4.8) or non-buffered YNB-Pro plates (pH 4.0) supplemented with LiCl, NaCl, or KCl as indicated ($t = TPS1$ terminator, pC = centromeric plasmid). Cells were grown at 30°C for 2 (control), 6 (LiCl) or 4 (NaCl, KCl) days. (c) Nomarski (left) and fluorescence (right) micrographs of BW31 cells expressing either N-terminally GFP-tagged *HsNHA2*, C-terminally GFP-tagged *HsNHA2* or *ScNha1*-GFP (expressed from pGFP-*HsNHA2t*, pGFP-*HsNHA2*, p*HsNHA2*-GFP or pNHA1-985GFP, respectively). Cells were grown in YNB-Pro (4% glucose) to the early exponential phase. The scale bar corresponds to 10 μm

antiporter(s) has never been measured directly in yeast cells.

In this work, we first optimized the functional expression of *HsNHA2* in *S. cerevisiae* cells and obtained a

highly valuable experimental model that we next used for in vivo determination of effects of *HsNHA2* mutations that alter its substrate specificity, transport activity, stability, or are among the single-nucleotide polymorphisms (SNP) in humans. In addition, for the first time, we demonstrate that the hydrophilic N-terminus (and negatively charged residues in this part of the protein) has a regulatory (inhibition) effect on *HsNHA2* activity. Altogether, our data suggest an allosteric link between the hydrophilic N-terminus and transmembrane core of the protein.

2 | RESULTS

2.1 | Optimization of *HsNHA2* expression in yeast cells

A eukaryotic cell model organism, the yeast *S. cerevisiae*, has been used for functional characterization of human proteins for a long time. Several mammalian Na^+/H^+ antiporters were also studied via their expression in *S. cerevisiae*,^{32,33} including *Homo sapiens* NHA2.^{4,6,23,31} In these studies, *HsNHA2* was expressed under the control of a strong promoter (*PGK1* or *TEF1*) from a multi-copy plasmid in a salt-sensitive strain (AB11c; *nha1 Δ ena1-4 Δ nhx1 Δ*). *HsNHA2* activity was then observed as a pH-dependent increase in tolerance to sodium or lithium, estimated by the growth of cells either in liquid media or on plates containing the corresponding salts.^{4,6,23,31} However, in our first experiment, we realized that using one of these previously made constructs (pTEF1-*HsNHA2*-HA), in which *HsNHA2* is expressed under the control of the *TEF1* promoter (Table 1⁴) is partially toxic for AB11c cells as well as for another strain, BW31, which only lacks the two plasma-membrane Na^+ exporters (*nha1 Δ ena1-4 Δ*). In both cases, cells expressing *HsNHA2* grew under non-stress conditions significantly slower than cells containing the empty vector (shown for the BW31 strain in Figure 1, control plates). Therefore, we next carefully examined and optimized the conditions of the expression of *HsNHA2* in *S. cerevisiae* (non-toxic for yeast cells) to obtain a valuable experimental model useful for the in vivo determination of *HsNHA2* transport activity. We constructed seven new plasmids (centromeric or multi-copy; Table 1), in which the *HsNHA2* was expressed under the control of a weak and constitutive *S. cerevisiae* *NHA1* promoter.³⁴ Four plasmids contained a GFP sequence added in frame either at the 5'- or 3'-ends of *HsNHA2* to confirm a plasma-membrane localization of *HsNHA2* in yeast cells (Table 1^{6,31}). Since the presence of a terminator behind any gene is important for mRNA export from the nucleus to the cytoplasm, as well as its stability and translation efficiency,³⁵ an

TABLE 1 Plasmids used in this study

Plasmid	Description ^a	Source/reference
YEp352	Multi-copy empty vector	19
pHsNHA2	<i>H. sapiens</i> NHA2 in YEp352	This work
pGRU1	Multi-copy empty vector with GFP	B. Daignan-Fornier, NCBI Acc. No. AJ249649
pHsNHA2-GFP	<i>H. sapiens</i> NHA2 in pGRU1	This work
pGFP- <i>HsNHA2</i>	N-terminally GFP tagged <i>HsNHA2</i> in YEp352	This work
pHsNHA2t	<i>H. sapiens</i> NHA2 with <i>TPS1</i> terminator in YEp352	This work
pGFP- <i>HsNHA2t</i>	N-terminally GFP tagged <i>HsNHA2</i> with <i>TPS1</i> terminator in YEp352	This work
pNHA1-985	<i>S. cerevisiae</i> NHA1-985 in YEp352	20
pNHA1-985GFP	<i>S. cerevisiae</i> NHA1-985 in pGRU1	20
pTEF1- <i>HsNHA2</i> -HA	<i>H. sapiens</i> NHA2 in p426TEF	4
pRS316	Centromeric empty vector	21
pC- <i>HsNHA2t</i>	<i>H. sapiens</i> NHA2 with <i>TPS1</i> terminator in pRS316	This work
pC-GFP- <i>HsNHA2t</i>	N-terminally GFP tagged <i>HsNHA2</i> with <i>TPS1</i> terminator in pRS316	This work
YEp352-ZrSTL1-TPS1t-kanMX	Plasmid for the expression of <i>Zygosaccharomyces rouxii</i> <i>STL1</i> gene downstream with the <i>TPS1</i> terminator	22

^a*ScNHA1* or *HsNHA2* were expressed under the control of *S. cerevisiae* *NHA1* promoter, except in pTEF1-*HsNHA2*-HA, in which TEF1 promoter was used.

efficient *S. cerevisiae* terminator *TPS1*³⁶ was added behind the *HsNHA2* cDNA in four versions of plasmids (Table 1). BW31 cells were transformed with all new plasmids, and we compared the level of cell salt tolerance provided by *HsNHA2* expressed from particular plasmids (Figure 1b). Salt tolerance was tested on YNB-Pro plates with the pH adjusted to 4.0 to ensure the necessary gradient of H⁺ for the transport activity of *HsNHA2*.⁴ Adjustment of the media to lower pH from approximately 4.8 to 4.0 with HCl accentuated the phenotypes on plates with salts described below (results obtained on non-adjusted YNB-Pro plates are not shown). Cells expressing empty vectors (YEp352, pRS316) or *S. cerevisiae* *Nha1* antiporter (non-tagged or tagged with GFP) were used as negative or positive controls, respectively. BW31 cells containing an empty vector (YEp352 or pRS316; Table 1) were highly sensitive to all three salts tested (LiCl, NaCl, KCl), while cells expressing the *ScNha1* antiporter were able to grow in the presence of LiCl, NaCl, and KCl (Figure 1b), as *ScNha1* is able to export all three cations from cells.²⁰ None of the constructs with *HsNHA2* improved the cell growth on KCl plates, which confirmed the previous results that *HsNHA2* is not transporting K⁺.^{4,30}

The expression of *HsNHA2* from new plasmids was not toxic for cells, as all transformants grew as well as cells containing empty vectors or expressing the yeast *Nha1* antiporter on control plates (and better than cells transformed with pTEF1-*HsNHA2*-HA) (Figure 1b). The level of *HsNHA2* expression from centromeric plasmids

(pC-*HsNHA2t*, pC-GFP-*HsNHA2t*) was too low to observe its activity, since cells with these plasmids grew similarly to cells with empty vectors (Figure 1b). On the other hand, the expression of *HsNHA2* under the control of the *ScNHA1* promoter from new multi-copy plasmids increased the cell tolerance to LiCl and NaCl, although they differed in the level of tolerance provided (Figure 1b). Cells expressing *HsNHA2* from pHsNHA2t or pHsNHA2-GFPt plasmids were more tolerant to salts than cells with the same constructs without the terminator (Figure 1b). Thus, the use of multi-copy plasmids with a weak *ScNHA1* promoter and *TPS1* terminator was the best for studying the transport properties of human *NHA2* expressed in yeast.

To consider various types of expression for the correct targeting of *HsNHA2* to the plasma membrane, we first compared the localization of GFP-tagged versions of *HsNHA2* in AB11c and BW31 cells, and realized that the lack of intracellular Nhx1 antiporter in the AB11c strain resulted in a higher intracellular stacking of GFP-*HsNHA2* than in BW31 cells (Figure S1). Thus, we subsequently only used the BW31 strain. As shown in Figure 1c, the GFP-tagging of *HsNHA2* at the C-terminus also resulted in a partial stacking of the antiporter in the endoplasmic reticulum (Figure 1c), and correspondingly, the tolerance of cells expressing *HsNHA2*-GFP was lower than that of cells with non-tagged *HsNHA2* or *HsNHA2* tagged with GFP at the N-terminus (Figure 1b). *HsNHA2* with a GFP tag at the N-terminus exhibited similar

plasma-membrane localization to ScNha1-GFP (Figure 1c). The expression of GFP-*HsNHA2* from a plasmid with a *TPS1* terminator (pGFP-*HsNHA2t*) resulted in a diminished level of intracellular fluorescent spots observed in cells containing pGFP-*HsNHA2* (Figure 1c, compare the upper two images).

Thus, from all these tested conditions, for the optimal functional expression of *HsNHA2* in yeast cells and further experiments, we selected the BW31 strain transformed either with the *pHsNHA2t* or pGFP-*HsNHA2t* plasmids.

2.2 | Point mutations of Pro246 modify the ion selectivity of the antiporter for Na⁺ and/or Li⁺ and its transport activity at pH 7.0

The membrane parts of Na⁺/H⁺ antiporters are highly conserved and are sufficient for ion exchange.^{20,25} In the last phylogenetic analysis, a minimal set of eight highly conserved positions in the protein core that are present in all CPAs was identified.² In *HsNHA2*, this motif contains, among others, proline 246 in TMS 6 and arginine 432 in TMS 12 (Figures 1a and S1). The replacement of an equivalent proline with a polar amino-acid residue (serine or threonine) in the homologous Na⁺, Li⁺/H⁺ antiporter Sod2-22 from *Zygosaccharomyces rouxii* resulted in an ability to recognize and transport K⁺ cations.³⁷ Thus, in the next part of this work, we tested how a substitution of P246 in *HsNHA2* can change its substrate specificity and transport activity (Figure 2). Proline 246 was replaced by site-directed mutagenesis either with glycine, a small hydrophobic amino acid (alanine) or polar residues (serine or threonine), and mutated versions were expressed in the BW31 strain from the corresponding *pHsNHA2t* or pGFP-*HsNHA2t* plasmids. Transformants were tested for their tolerance to LiCl, NaCl or KCl at pH 4.0 or 7.0 in comparison with cells transformed with the empty vector or expressing the native *HsNHA2* antiporter (Figure 2a). None of the mutated versions improved the tolerance of cells to KCl (not shown), but we observed that their ability to provide cells with tolerance to LiCl or NaCl within the pH range 4.0–7.4 was different from the native antiporter (Figure 2a,e). The GFP-tagging had no effect on the substrate specificity of mutated versions (cf. below), but it slightly enhanced the phenotypes observed as cell salt tolerance on plates (compare Figures 2a and S3A). All four mutated versions were localized to the plasma membrane (Figure 2c), like the native GFP-*HsNHA2* (Figure 1c), and similar amounts of proteins in cells were detected by immunoblot for all of them (Figure 2d).

As expected, the presence of the native antiporter only increased cell tolerance to sodium and lithium at pH 4.0 (when there is a high H⁺ gradient across the membrane), but not at pH 7.0 (Figure 2a). The P246G substitution resulted in an almost inactive antiporter, as cells with this mutated version grew only slightly better in the presence of salts than cells containing the empty vector (Figure 2a). The P246A mutation resulted in an antiporter which was able to transport Li⁺ better than the native antiporter, but its ability to improve the NaCl tolerance was much lower than that of the native *HsNHA2* (Figure 2a). In contrast, Pro246 replaced with threonine resulted in an antiporter with the opposite substrate preferences to the P246A version, that is, transporting lithium worse and sodium better than the native *HsNHA2* (Figure 2a). Finally, *HsNHA2* with the P246S mutation provided a better tolerance of cells to both cations compared to the native *HsNHA2* (Figure 2a).

Interestingly, and in contrast to the native antiporter, *HsNHA2* harboring the point mutations P246A/S/T also exhibited activity at a higher external pH than 4.0. They improved the tolerance of BW31 cells to both cations on non-buffered plates with the pH adjusted to 7.0 (Figure 2a), where the P246T version provided the most robust growth (Figure 2a). In the growth test shown in Figure 2e, we verified this observation on plates with buffered media (cf. Section 5). On these plates, extracellular pH should not change with the growth of cells, as in Figure 2a. It is evident that under these conditions, each of the three P246A/T/S versions was able to improve the tolerance of cells to LiCl within the pH range 4.0–7.4, and the P246T/S versions also to NaCl (Figure 2e). Note that in contrast to P246A/S, the ability of the P246T version to improve the tolerance to LiCl increased with increasing extracellular pH (Figure 2e). This drop test also confirmed the decreased activity of the P246G version in comparison with the native *HsNHA2*, in which Li⁺ and Na⁺ transport activity was only observable on plates with low pH 4.0 (Figure 2e or a).

Next, the differences in capacity to transport Na⁺ cations observed in drop tests (Figure 2a,e) were verified by sodium loss measurements at pH 4.0 (Figure 2b) from sodium-preloaded cells (cf. Section 5). During the experiment, the intracellular concentration of Na⁺ also slightly decreased in control cells without any antiporter (Figure 2b, empty vector), but significantly higher efflux was observed in cells with the native *HsNHA2* (Figure 2b). In accordance with the drop tests, the amounts of sodium lost from cells expressing the *HsNHA2* antiporter with the P246A or P246G mutation were lower than from cells with the native *HsNHA2*, but higher than from cells with the empty vector (Figure 2b). On the other hand, the P246S, and especially the P246T

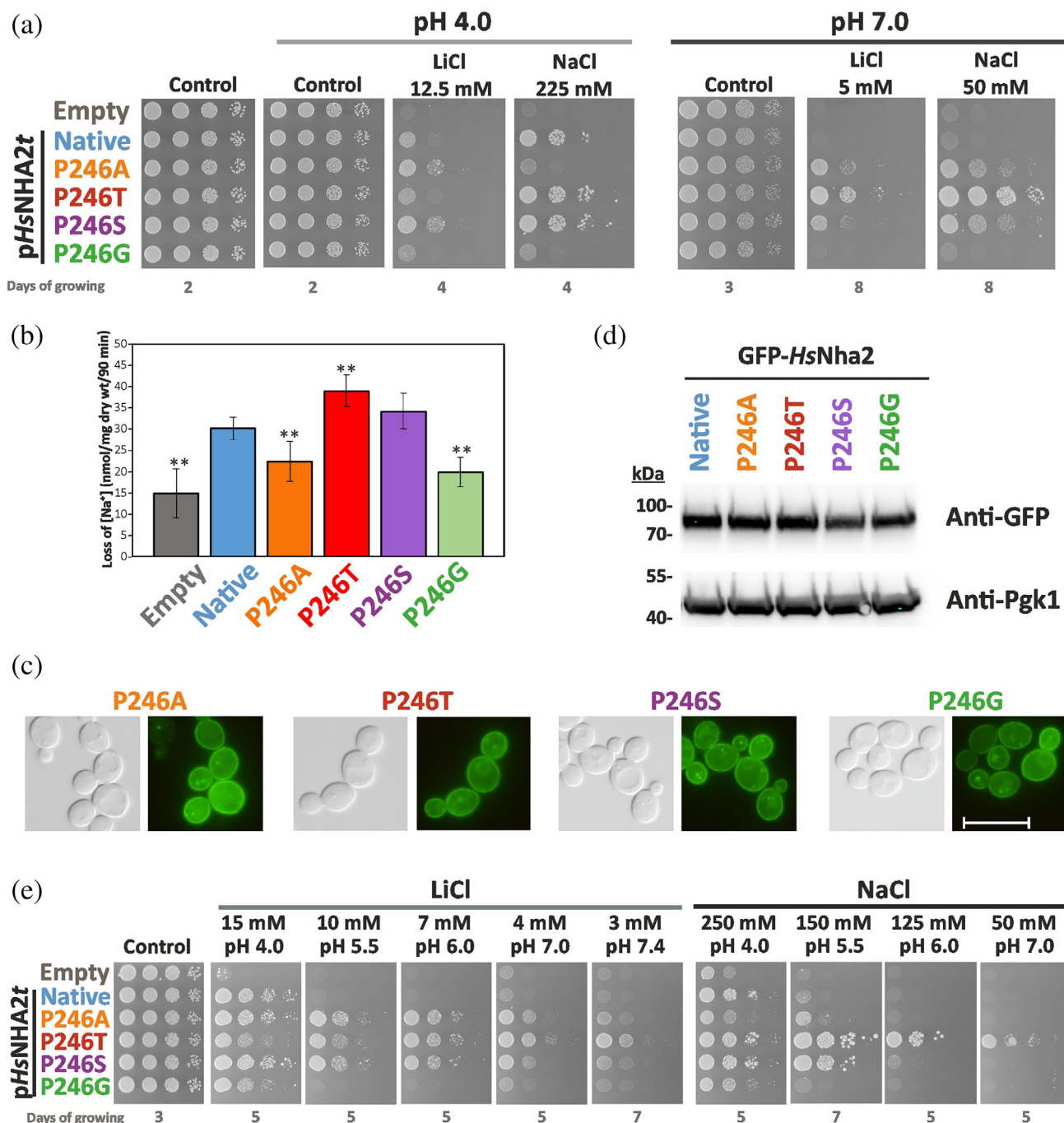


FIGURE 2 Characterization of *HsNHA2* with point mutations at proline 246. (a) Salt tolerance of *S. cerevisiae* BW31 cells containing empty vector or expressing native *HsNHA2* or one of four *HsNHA2* versions with single point mutations P246A, T, S or G from *pHsNHA2t* plasmid. Cells were grown on YNB-Pro or non-buffered YNB-Pro plates with pH adjusted to 4.0 or 7.0 and supplemented with LiCl or NaCl as indicated. Plates were incubated at 30°C and photographed on the indicated day. (b) Loss of Na⁺ from same cells as described in (a). Cells were grown in YNB-Pro media, preloaded with Na⁺, transferred to Na⁺-free incubation buffer at pH 4.0 and changes in the intracellular Na⁺ content were estimated as described in Section 5. Columns show the amount of Na⁺ lost from cells within 90 min. Data represent the mean of at least 5 replicate values ± SD. Significant differences compared to cells expressing the native *HsNHA2* are indicated with asterisks (***p* < .01). Localization (c) and immunodetection (d) of N-terminal GFP-tagged *HsNHA2* with single point mutations at Pro246. BW31 cells expressing variants of GFP-*HsNHA2* from *pGFP-HsNHA2t* were grown in YNB-Pro (4% glucose) to the exponential phase and observed under a fluorescence microscope (c, right). A Nomarski prism was used for whole-cell imaging (c, left). In (d), protein extracts of cells were prepared as described in Section 5, subjected to SDS-PAGE (10% gel) and transferred to a nitrocellulose membrane. Native GFP-*HsNHA2* and its variants were detected with an anti-GFP antibody. The membrane was reprobbed and incubated with an anti-Pgk1 antibody to verify the amount of loaded proteins. (e) Activity of mutated *HsNHA2* antiporters at various extracellular pH was determined by growth of cells on YNB-Pro plates buffered to various pH levels (4.0–7.4) and supplemented with LiCl or NaCl as indicated. Images were taken on the indicated day of incubation at 30°C

mutation increased *HsNHA2* transport activity for Na^+ . The amount of sodium lost from these cells was significantly higher than from cells with the native antiporter (Figure 2b). Since the localization and amounts of proteins did not change with the P246 substitutions (Figure 2c,d), sodium loss measurements fully reflected the sodium transport capacity of the particular mutated versions observed as differences in growth on plates with NaCl (Figure 2a,e).

All these data identified proline 246 as a crucial residue involved in the ability to recognize and transport particular substrates (ion selectivity), most likely also influencing the capacity to transport protons, as the pH profile of *HsNHA2* transport activity changed, especially when the polar-branched amino acid threonine was at this position.

2.3 | *HsNHA2* with substitutions at Pro246 are less sensitive to phloretin inhibition

The activity of *HsNHA2* is insensitive to amiloride (a hallmark of plasma-membrane NHE antiporters), and sensitive to phloretin,³⁰ even when it is expressed in yeast cells.⁶ Phloretin (a flavonoid abundant in apples) is a highly flexible molecule with the ability to bind to biological macromolecules. It has interesting pharmacological and pharmaceutical potential due to its antimicrobial, antioxidant, anti-inflammatory, and anticancer activities.³⁸ The mechanism of *HsNHA2* inhibition by phloretin is unclear. To determine whether mutations of P246 change the sensitivity of the antiporter to phloretin, we tested the growth of cells expressing the native, or either of the four antiporters mutated at proline P246, on plates supplemented with 15 mM LiCl or 250 mM NaCl and increasing concentrations of phloretin (Figure 3).

In accordance with previous results⁶, the ability of the native *HsNHA2* to improve LiCl tolerance at pH 4.0 of yeast cells highly decreased in the presence of phloretin (Figure 3). Here we also demonstrate the same effect of phloretin on Na^+ transport activity (Figure 3). Remarkably, the inhibition effect of phloretin decreased when proline 246 was replaced with alanine/glycine or even disappeared when serine or threonine was at this position (Figure 3). BW31 cells transformed with these versions of *HsNHA2* grew on plates with LiCl or NaCl and phloretin very similarly to when the inhibitor was not present (Figure 3).

These results reinforced the importance of proline 246 for the proper activity of *HsNHA2*. They also indicate that this residue could take part in a mechanism of inhibition mediated by phloretin.

2.4 | Swapping E215 and R432 results in a Li^+ -specific antiporter that is also active at higher pH

As was mentioned above, R432 is one of the eight highly conserved amino acids of the whole CPA family, and it was predicted to potentially form a salt bridge with E215 in TMS 5 (Figure 1a).² To experimentally prove the importance and function of these two titratable residues, we prepared three mutated versions of *HsNHA2* in which we either introduced the opposite charge at these positions (E215R or R432E versions) or we swapped these two residues (E215R + R432E double mutant). The effect of mutation(s) on the transport properties of *HsNHA2* was tested similarly as above.

The single-mutated versions of the antiporter, E215R or R432E, were non-functional (Figure 4a). Cells transformed with *pHsNHA2t* (E215R) or *pHsNHA2t* (R432E) plasmids did not grow in the presence of NaCl or LiCl

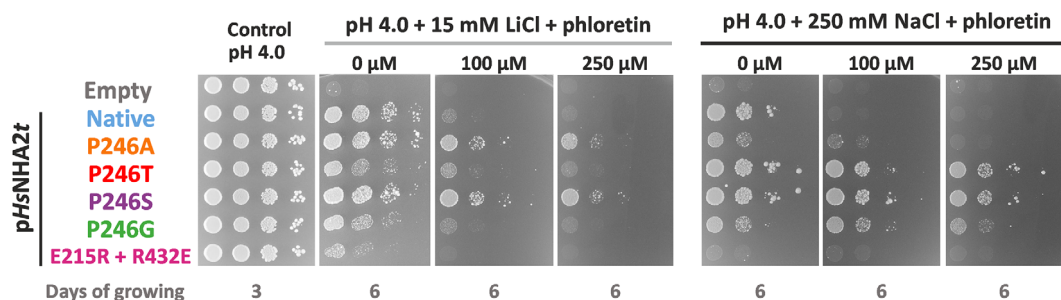


FIGURE 3 *HsNHA2* variants of proline 246 are less sensitive to phloretin inhibition. *S. cerevisiae* BW31 cells containing empty vector or expressing native *HsNHA2* or *HsNHA2* versions with point mutations P246A, T, S or G or the double mutation E215R + R432E from *pHsNHA2t* plasmid, as indicated, were used in this experiment. The inhibition of mutated *HsNHA2* versions by phloretin was determined by the growth of cells on non-buffered YNB-Pro plates with the pH adjusted to 4.0 and supplemented with LiCl or NaCl, and with or without phloretin at the indicated concentrations. Plates were incubated at 30°C for 3 (controls) or 6 days (phloretin)

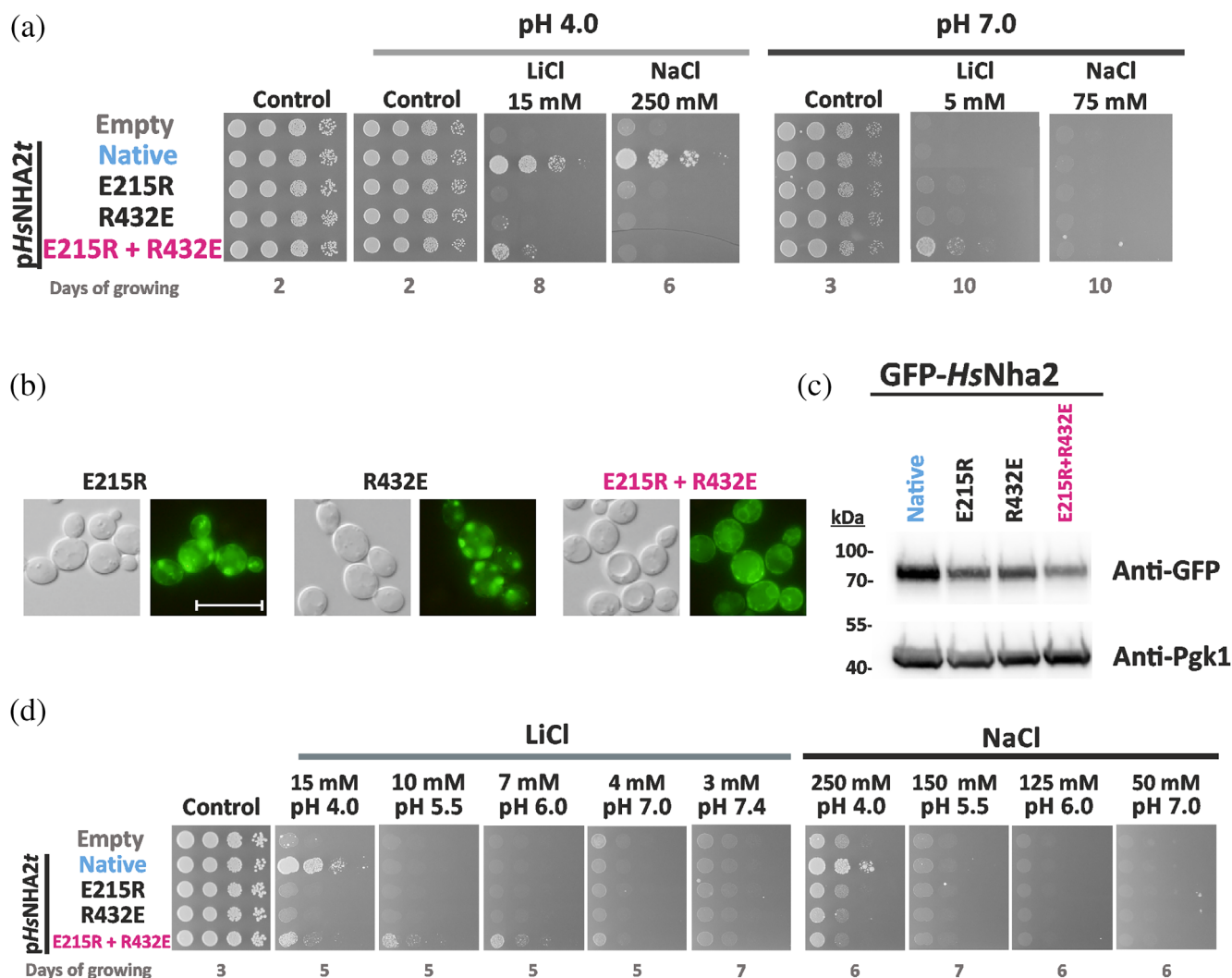


FIGURE 4 Characterization of *HsNHA2* with mutations of residues forming a putative salt bridge. (a) Salt tolerance of *S. cerevisiae* BW31 cells containing empty vector or expressing native *HsNHA2* or its mutated versions (E215R, R432E or E215R + R432E) from *pHsNHA2t* plasmid. Cells were grown on YNB-Pro (pH approx. 4.8) or non-buffered YNB-Pro plates with the pH adjusted to 4.0 or 7.0 and supplemented with LiCl or NaCl as indicated. Plates were incubated at 30°C and photographed on the indicated day. Localization (b) and immunodetection (c) of N-terminal GFP-tagged *HsNHA2* mutated versions E215R, R432E or E215R + R432E. Cells were grown in YNB-Pro (4% glucose) to the exponential phase and observed under a fluorescence microscope (b, right). A Nomarski prism was used for whole-cell imaging (b, left). The scale bar corresponds to 10 μ m. In (c), protein extracts from the same cells as in (b) (with cells expressing native GFP-*HsNHA2* as a control) were prepared as described in Section 5, subjected to SDS-PAGE (10% gel) and transferred to a nitrocellulose membrane. GFP-*HsNHA2* was detected with an anti-GFP antibody. The membrane was reprobed and incubated with an anti-Pgk1 antibody to verify the amount of loaded proteins. (d) Activity of mutated *HsNHA2* antiporters at various extracellular pH levels determined by growth of cells on YNB-Pro plates buffered to various pH levels (4.0–7.4) and supplemented with LiCl or NaCl as indicated. Images were taken on the indicated day of incubation at 30°C

(at both pHs, 4.0 or 7.0), just like cells containing the empty vector (Figure 4a). On the other hand, swapping these two residues led to a functional antiporter, however, with substrate specificity limited to Li^+ cations. At both of pH levels, cells expressing *HsNHA2* (E215R + R432E) were only able to grow on plates with LiCl, but not with NaCl (Figure 4a). Similar results were observed in a drop test with cells expressing the same mutated versions, but tagged with GFP at the N-terminus (Figure S3B).

The loss of function of the two single-mutated versions most likely resulted from their mislocalization in intracellular compartments, observed as fluorescent spots inside cells (Figure 4b). In contrast, the double-mutated E215R + R432E version tagged with GFP was partially targeted to the plasma membrane and partially observed in the perinuclear ER (Figure 4b). The level of proteins expressed in cells checked by immunoblotting revealed that all three mutated variants were present in cells in lower amounts than the native antiporter (Figure 4c).

Since all proteins are expressed under the same conditions (plasmid, promoter, terminator), it indicates that these mutations affected the structure, stability, and plasma-membrane targeting of *HsNHA2*.

The drop test on plates with salts and pH buffered to various values (Figure 4d) confirmed the lithium substrate specificity of the E215R + R432E version. In contrast to the native antiporter, it was able to improve the LiCl tolerance of cells not only at pH 4.0, but also at higher pH, up to 6.0 (Figure 4d). Nevertheless, in contrast to P246 variants, phloretin inhibited the Li⁺ transport ability of the double mutant E215R + R432E, as observed for the native *HsNHA2* (Figure 3).

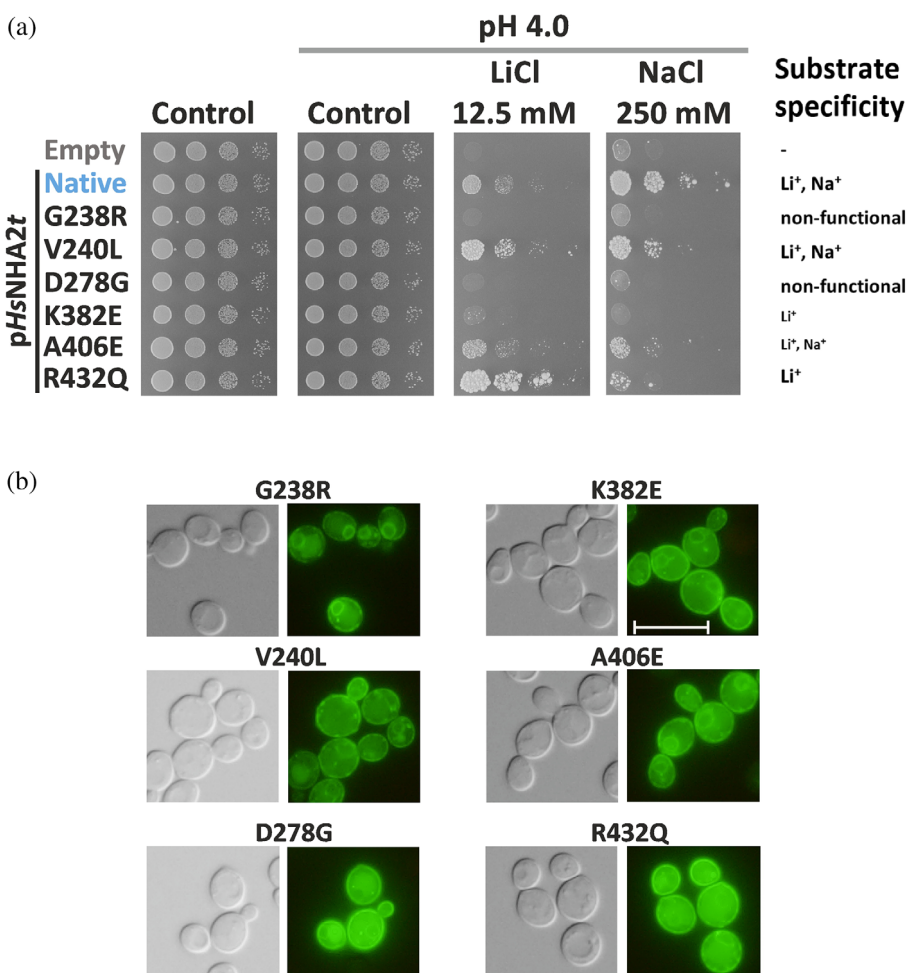
All these results confirmed E215 and R432 to be crucial residues for *HsNHA2* functionality. The transport activity of the antiporter with the E215R mutation in TMS 5 could be restored by introducing a second mutation R432E in TMS 12 (Figures 1, S1, and 8). Thus, we experimentally confirmed that in the full version of *HsNHA2* (containing the hydrophilic N-terminus), these two residues are spatially close to each other with a salt bridge between them. The interaction between these two residues is important for the structural integrity of the protein.

2.5 | Validation of the system for studying the effect of SNPs in *HsNHA2*

As was mentioned above, *HsNHA2* is associated with a growing list of various pathologies. For this reason, we think that our optimized expression system of *HsNHA2* in yeast cells could be useful in the future for the characterizing the effects of a broad range of mutations that are present in human genomes. To test this possibility, we selected six point mutations (G238R, V240L, D278G, R432Q, K382E, and A406E) that belong to known human SNPs from patients.³⁹ The positions of these residues in *HsNHA2* are shown in Figures 1a, S1, and 8b,e. Mutated versions were prepared by site-directed mutagenesis and expressed from *pHsNHA2t* or *pGFP-HsNHA2t* plasmids in BW31 cells, and we tested the tolerance of cells to LiCl and NaCl at pH 4.0 (Figures 5a and S4). The localization of the corresponding GFP-tagged versions was observed by fluorescence microscopy (Figure 5b).

All six mutations influenced the transport properties of *HsNHA2*, but to various extents. The mutation V240L resulted in an antiporter with a preference for transporting Li⁺ over Na⁺, while the R432Q or K382E versions narrowed the substrate specificity of the antiporter only

FIGURE 5 Phenotypes of SNPs of *HsNHA2*. (a) Salt tolerance of *S. cerevisiae* BW31 cells containing empty vector or expressing native *HsNHA2* or one of six *HsNHA2* mutated versions—G238R, V240L, D278G, K382E, A406E, and R432Q from the *pHsNHA2t* plasmid. Cells were grown on YNB-Pro or non-buffered YNB-Pro plates with pH adjusted to 4.0 and supplemented with LiCl or NaCl as indicated. Growth was monitored for 2 (controls) or 7 (LiCl or NaCl) days at 30°C. (b) Localization of N-terminal GFP-tagged *HsNHA2* versions. BW31 cells expressing GFP-*HsNHA2* with single point mutations as in (a) from *pGFP-HsNHA2t* were grown in YNB-Pro (4% glucose) to the exponential phase and observed under fluorescence microscope (b, right). A Nomarski prism was used for whole-cell imaging (b, left). The scale bar corresponds to 10 μm



for Li^+ (Figure 5a; for K382E cf. also Figure S4). The point mutation A406E resulted in a less active antiporter for both cations, as cells with this mutated antiporter grew worse in the presence of both salts than cells with the native one (Figure 5a). Neither of the mutated versions G238R or D278G were functional, because in the presence of salts, cells with these antiporters grew very similarly to cells with the empty vector (Figure 5a). However, the non-functionality of G238R resulted from misfolding of the antiporter (stacking in the ER; Figure 5b), while for D278G, which was localized in the plasma membrane (Figure 5b), it was instead due to the effect of the mutation on activity (the mechanism of transport). The fluorescence in cells expressing GFP-*HsNHA2* with V240L, K382E, A406E, or R432Q was also observed predominantly in the plasma membrane (Figure 5b).

These results confirmed that in the future our expression system may provide an efficient screening of the effects of mutations present in *HsNHA2* versions associated with pathologies or for the large-scale testing of various compounds that activate/inhibit the *HsNHA2* activity.

2.6 | Amino acids 1–40 of the hydrophilic N-terminus inhibit the transport activity of *HsNHA2*

HsNHA2 and its homologs from other mammals possess an unusually long hydrophilic N-terminus (about 82 aa, Figure S1), which is not present in the NHE clade.^{2,23} The structure of the N-terminus is predicted to be disordered (Alpha-fold prediction Q86UD5).²⁴ In the above drop test experiments, we always noticed that N-terminally GFP-tagged versions of *HsNHA2* provided BW31 cells with a higher tolerance to LiCl and NaCl (Figures S3–S5) than the corresponding variants without the tag (Figures 2, 4, and 5), even though the expression conditions were the same. This observation indicated that GFP-tagging somehow activated *HsNHA2*, and that the hydrophilic N-terminal part of the protein may play a role in the regulation of the transport activity of *HsNHA2*. In addition, the cryo-EM structure of bison NHA2 truncated by 69 amino acids from the N-terminus indicated the presence of an unusual short helical segment (corresponding to amino acids 70–79) prior to TMS 1.²³

To understand the role of the N-terminus in *HsNHA2*'s function, we constructed a series of step-by-step truncated *HsNHA2* versions, ranging from the complete antiporter down to the shortest version lacking the first 90 amino acids (Figure S1). In eight newly prepared constructs of *HsNHA2*, codons for amino acids at positions 20, 40, 60, 70, 75, 80, and 90 were replaced by the

start codon ATG for methionine. Truncated *HsNHA2* versions were expressed in BW31 cells, and tested for their properties as above (Figure 6). For each version, a corresponding N-terminal GFP-tagged construct was used to test the localization and level of expression of the encoded protein (Figure 6c,d).

The lack of the first 40 amino acids had no effect on *HsNHA2* transport properties. Cells with $\Delta 1$ –20 and $\Delta 1$ –40 truncated versions exhibited the same salt tolerance as the native *HsNHA2* (Figure 6a). The lack of the first 40 amino acids also did not change the Na^+ -efflux activity of the antiporter (Figure 6b). On the other hand, cells expressing $\Delta 1$ –50, $\Delta 1$ –60, or $\Delta 1$ –70 versions grew better on LiCl and NaCl plates than cells expressing the native antiporter (Figure 6a). This suggested that truncation of the first 50–70 aa increased the activity of the antiporter, which we confirmed by measurements of Na^+ -efflux activity (Figure 6b). Notably, the amount of Na^+ lost from cells expressing the $\Delta 1$ –50, $\Delta 1$ –60, or $\Delta 1$ –70 *HsNHA2* variants was double that of the native antiporter or $\Delta 1$ –40 version (Figure 6b). Truncations longer than 75 amino acids resulted in less efficient transporters, as they provided cells with lower LiCl and NaCl tolerance than the native antiporter, and the removal of 90 amino acids resulted in a non-functional protein (Figure 6a). Truncations up to 70 amino acids did not influence the plasma-membrane localization of the antiporter (Figure 6b). In contrast, the fluorescence signal in cells with the $\Delta 1$ –75, $\Delta 1$ –80, or $\Delta 1$ –90 GFP-*HsNHA2* antiporters was predominantly observed in intracellular compartments (Figure 6c). Thus, these versions were probably not folded properly, which led to their mislocalization. Neither of these truncated versions was able to improve the salt tolerance of BW31 cells on plates with pH 7.0 (results not shown), which means that the dependency on the H^+ gradient of *HsNHA2* did not change with N-terminal truncations.

The immunodetection of truncated versions (Figure 6d) showed that the signal of the GFP-*HsNHA2* proteins gradually decreased with larger truncations of the N-terminus, being the weakest for the last three ($\Delta 1$ –70, $\Delta 1$ –80, or $\Delta 1$ –90). This indicates that the N-terminus is not only important for the regulation of transport activity, but also for the stability of the protein and/or its trafficking to the plasma membrane. Interestingly, in contrast to the point mutations studied above (localized within the TMS), the GFP-tagging decreased the ability of truncated *HsNHA2* to improve the tolerance of cells to LiCl, but the provided tolerance to NaCl was enhanced with a truncation longer than 40 aa, as with non-tagged antiporters (compare Figure 6a and S5).

Although the protein signals detected by immunoblotting for the $\Delta 1$ –50, $\Delta 1$ –60, or $\Delta 1$ –70 versions were much lower than that for the native antiporter

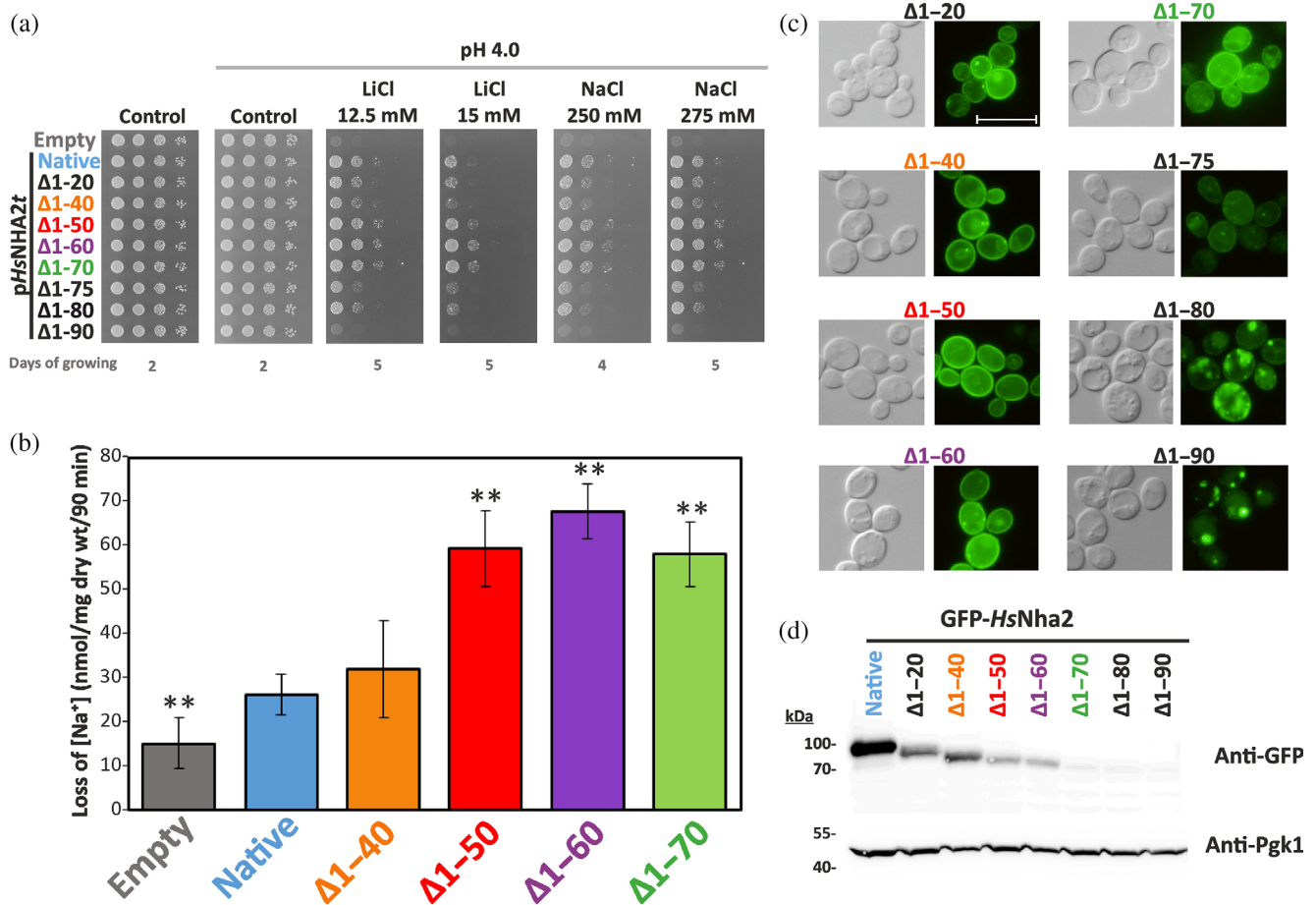


FIGURE 6 Hydrophilic N-terminus of *HsNHA2* plays inhibitory role. (a) Salt tolerance of *S. cerevisiae* BW31 cells containing empty vector or expressing native or N-terminally truncated *HsNHA2* versions from plasmids derived from *pHsNHA2t*. Cells were grown on YNB-Pro (pH approx. 4.8) or non-buffered YNB-Pro plates with pH adjusted to 4.0 and supplemented with LiCl or NaCl as indicated. Plates were incubated at 30°C and photographed on the indicated day. (b) Loss of Na^+ from BW31 cells mediated by N-terminal truncated *HsNHA2* versions. Cells were grown in YNB-Pro media, preloaded with Na^+ , transferred to Na^+ -free incubation buffer at pH 4.0, and changes in the intracellular Na^+ content were estimated as described in Section 5. Columns show the amount of Na^+ lost from cells within 90 min. Data represent the mean of at least 3 replicate values \pm SD. Significant differences compared to cells expressing the native *HsNHA2* are indicated with asterisks (** $p < .01$). Localization (c) and immunodetection (d) of N-terminal GFP-tagged truncated *HsNHA2* versions. BW31 cells expressing variants of GFP-*HsNHA2* with truncated N-terminus from plasmids derived from *pGFP-HsNHA2t* were grown in YNB-Pro (4% glucose) to the exponential phase and observed under a fluorescence microscope (c, right). A Nomarski prism was used for whole-cell imaging (c, left). The scale bar corresponds to 10 μm . In (d), protein extracts from the same cells as in (c) (with cells expressing native GFP-*HsNHA2* as a control) were prepared as described in Section 5, subjected to SDS-PAGE (10% gel) and transferred to a nitrocellulose membrane. GFP-*HsNHA2* variants were detected with an anti-GFP antibody. The membrane was reprobbed and incubated with an anti-Pgk1 antibody to verify the amount of loaded proteins

(Figure 6d), these GFP-non-tagged versions exhibited at least double the Na^+ efflux activity (Figure 6b). Moreover, truncation of the N-terminus of 50 aa in GFP-*HsNHA2* also resulted in an increased Na^+ efflux activity in comparison with the native version of GFP-*HsNHA2* (57 ± 5 nmol Na^+ /mg dry wt/90 min vs. 35 ± 6 nmol Na^+ /mg dry wt/90 min, respectively). Since we observed this phenomenon in yeast cells, which may lack some regulatory mechanisms or protein interactions that regulate the activity of *HsNHA2* in mammalian cells,¹² the first 40–50 amino acids of the protein appears to allosterically auto-inhibit *HsNHA2* activity.

2.7 | Conserved charged amino acids in the hydrophilic N-terminus of *HsNHA2* are important for its activity

It was found that in the hydrophilic N-terminus of the Na^+/HCO_3^- co-transporter, the presence of charged (positively as well as negatively) residues is essential to fulfilling the auto-inhibitory function of the transporter.⁴⁰ To corroborate the role of the N-terminus in the regulation of *HsNHA2* activity, we compared the sequences of unique homologs of *NHA2* from various metazoan species (Figure 7a). In the important region revealed above

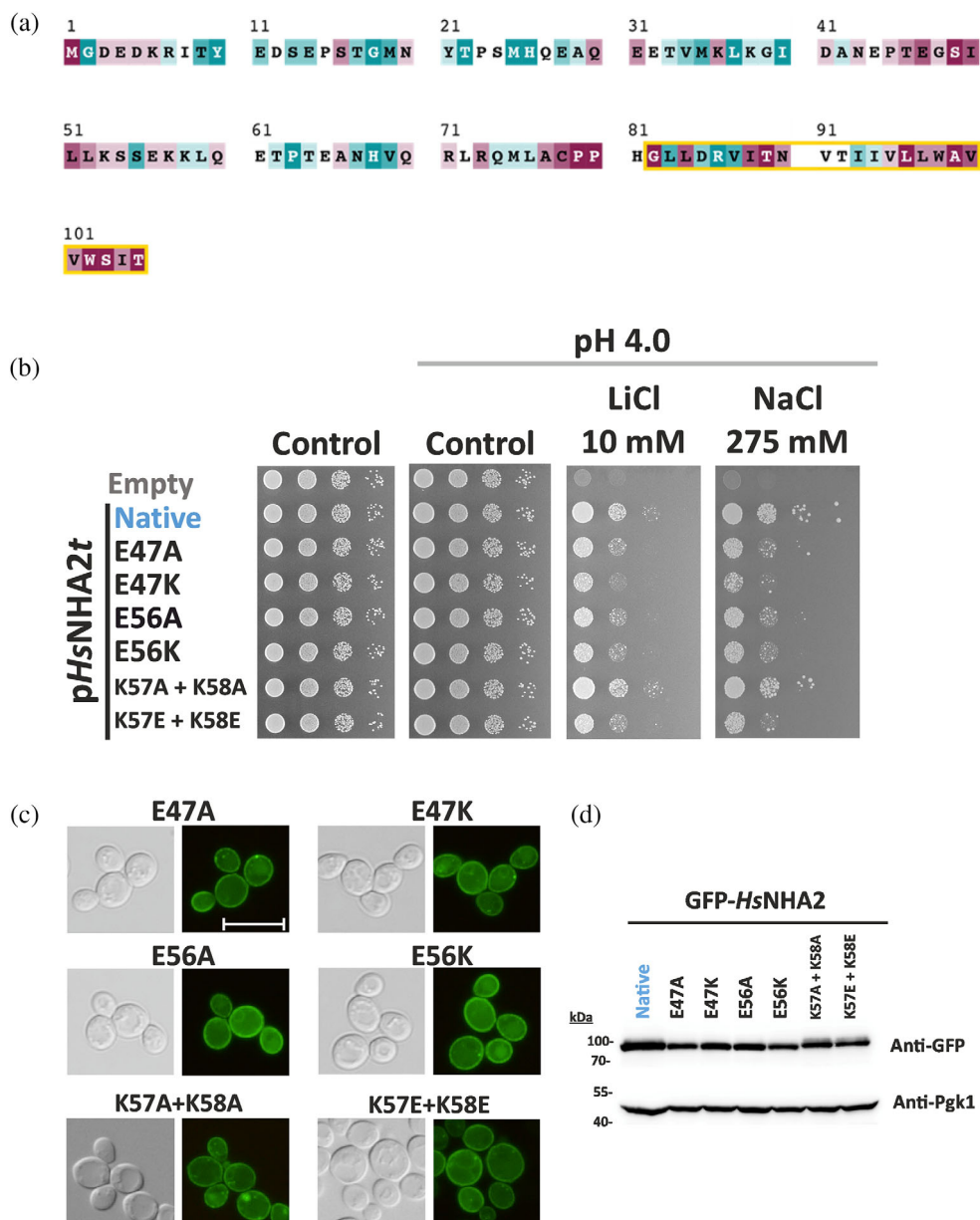


FIGURE 7 Charged residues in *HsNHA2* hydrophilic N-terminus are important for transport activity. (a) Evolutionary conservation analysis of *HsNHA2* N-terminus. *HsNHA2* N-terminal residues 1-to-105 colored based on ConSurf server evolutionary conservation scale, with cyan to maroon representing variable to conserved amino acids, respectively. The position of the unique N-terminal TMS is highlighted with a yellow box. The conservation analysis was conducted using *HsNHA2* N-terminal amino acids. A total of 99 unique sequences were collected by HMMER from the UniRef90 database with sequence identity ranging from 35 to 95% and an *E*-value of at least 0.00001. (b) Salt tolerance of *S. cerevisiae* BW31 cells containing empty vector or expressing native *HsNHA2* or one of six *HsNHA2* mutated versions E47A, E47K, E56A, E56K, K57A + K58A, or K57E + K58E from *pHsNHA2t*. Cells were grown on YNB-Pro or non-buffered YNB-Pro plates with the pH adjusted to 4.0 and supplemented with LiCl or NaCl as indicated. Plates were incubated at 30°C for 2 (controls) or 5 days (salts). Localization (c) and immunodetection (d) of N-terminal GFP-tagged *HsNHA2* mutated versions as in (b). BW31 cells expressing variants of GFP-*HsNHA2* from the *pGFP-HsNHA2t* were grown in YNB-Pro (4% glucose) to the exponential phase and observed under a fluorescence microscope (c, right). A Nomarski prism was used for whole-cell imaging (c, left). The scale bar corresponds to 10 μ m. In (d), protein extracts from the same cells as in (c) were prepared as described in Section 5, subjected to SDS-PAGE (10% gel) and transferred to a nitrocellulose membrane. GFP-*HsNHA2* variants were detected with an anti-GFP antibody. The membrane was reprobed and incubated with an anti-Pgk1 antibody to verify the amount of loaded proteins

(amino acids 40–70), we identified four charged residues (3 of them highly conserved; Figure 7a): negatively charged glutamates 47 and 56, and positively charged

lysines at positions 57 and 58, and we estimated their possible role in *HsNHA2* activity. We replaced these amino acids with neutral alanine or with an amino acid

with the opposite charge. The resulting six mutated versions of *HsNHA2* (E47A/K, E56A/K, K57A + K58A, K57E + K58E) were tested for their ability to improve the salt tolerance of BW31 cells at pH 4.0 in comparison with the native antiporter (Figure 7a). Fluorescence microscopy of GFP-tagged versions revealed that none of these mutations changed the plasma-membrane localization of the antiporter (Figure 7c), or the amount of proteins in cells (Figure 7d).

The drop test (Figure 7b) showed that both glutamate residues E47 and E56 are important for the antiporter's activity. Their replacement with alanine resulted in antiporters with a lower ability to improve the lithium and sodium tolerance of cells, and their replacement with an amino-acid with the opposite charge (lysine) emphasized this phenotype (Figure 7b). The replacement of K57 and K58 with alanines did not affect the antiporter's function, but negatively charged glutamates at these two positions also resulted in an antiporter with decreased activity (Figure 7b).

In summary, these experiments revealed a new role of the N-terminus in the regulation of *HsNHA2* activity and identified four charged amino-acid residues in the N-terminus as crucial for determining *HsNHA2* transport activity.

3 | DISCUSSION

As a unicellular eukaryotic organism, the yeast *S. cerevisiae* plays a key role in fundamental scientific research in exploring molecular aspects of cellular processes. Thanks to the identification of human orthologs to yeast proteins, including proteins related to human pathologies, yeast is widely used as a simplified cellular model of human diseases.⁴¹ The heterologous expression of human proteins in yeast cells also provides valuable information about the structure of human proteins and their functional domains.⁴² We optimized the expression of the human Na^+/H^+ antiporter NHA2 in yeast cells to be stable, functional, at a non-toxic level for cells, and with proper targeting to the plasma membrane (Figure 1). For the first time, we set the conditions and methodology for in vivo measurements of its Na^+ transport activity (Figures 2 and 6). Using this system enabled us to identify several as-yet unknown residues crucial for *HsNHA2* substrate specificity and transport activity (Figures 2, 4, 5, and 7), and to discover a possible auto-inhibitory role of the hydrophilic N-terminal segment (Figures 6 and 7), which appears to allosterically regulate transmembrane ion transport. Our experimental model is also a key tool for better understanding the molecular causes of pathologies related to single-nucleotide

polymorphism of *HsNHA2*, and to screen for putative modifiers, including drugs, which could alter *HsNHA2* activity (similarly as is shown in Figures 5 and 3, respectively).

All Na^+/H^+ antiporters seem to share a similar transmembrane topology, known as the NhaA fold, organized into two functional domains—a dimerization domain and a conserved core domain encapsulating the ion-binding site.^{43,44} According to recently resolved N-terminally truncated cryoEM structures of two NHA2 proteins (human [PDB 7B4L; Figure 8a], bison²³), the antiporter consists of 14 TMS, instead of the 13 TMS observed in mammalian NHE Na^+/H^+ exchangers^{45,46} and the prokaryotic NhaP1, NapA and NhaP antiporters^{47–50} or the 12 TMS in *Escherichia coli* antiporter NhaA.⁴³ *HsNHA2* possesses a long hydrophilic N-terminus that resides in the cytosol (Figures 1a and S1), which is followed by the first transmembrane helix corresponding to amino acids 82–105 (Figures 7a and 8a). Predicted to be unstructured, the hydrophilic N-terminal part preceding TMS1 is not present in both resolved NHA2 structures that were recently released (Protein Data Bank 7B4M or 7B4L²³). Specifically, in structural studies of bison NHA2, the protein was shortened of 69 amino acids at the N-terminus to reduce predicted disorder.²³ We have found that this region is important for the regulation of *HsNHA2* activity (Figure 6). Our data show that, in *HsNHA2*, molecular dissection of this region (aa 1–70) neither affected protein localization (Figure 6c) nor substrate specificity (Figure 6a). However, truncation of the first 50–70 aa from the N-terminus provided cells with higher tolerance to LiCl and NaCl (Figure 6a) and resulted in increased Na^+ -transport activity (Figure 6b). The activity of various Na^+/H^+ antiporters, members of the CPA1 clade, was found to be mainly regulated via their large C-terminal hydrophilic domains. A number of phosphorylation sites and binding sites that interact with regulatory proteins were found in these C-terminal segments.^{3,20,25,51} Nevertheless, our results revealed a novel and unique auto-inhibitory function of the N-terminus among human Na^+/H^+ antiporters. So far, an auto-inhibitory role of the hydrophilic N-terminus has been described in some other transporters, for example, the human Ca^{2+} and Mn^{2+} transporter TMEM165⁴² or $\text{Na}^+/\text{HCO}_3^-$ co-transporter NBCe1-B,⁴⁰ plant $\text{Ca}^{2+}/\text{H}^+$ antiporters⁵² or yeast vacuolar Na^+ , K^+/H^+ antiporter Vnx1.⁵³

The N-terminus of *HsNHA2* is poorly conserved except for the region between amino acids 45 and 60 (Figure 7a). We identified two glutamates (E47, E56) and two lysines (K57, K58) within this region as important residues for *HsNHA2* activity (Figure 7b), but not essential for the protein's stability (Figure 7d) or its

localization in the plasma membrane (Figure 7c). In particular, the replacement of these residues with an amino acid with the opposite charge resulted in *HsNHA2* with a decreased capacity to transport both its substrates, Li^+ and Na^+ (Figure 7b).

In bison *NHA2* $\Delta\text{N1-69}$, the TMS1 (aa 86–106) formed a unique homodimer interface with a large intracellular gap between the protomers, which closes in the presence of phosphoinositol lipids, and the lipid-compact form was more active.²³ Our results confirm that truncations larger than 75 amino acids in *HsNHA2* in the immediate proximity of TMS1 (aa 82–105; Figure 7a) led to the loss of function of the antiporter (Figure 6a), most likely due to protein misfolding, and consequently mislocalization (Figure 6c). The N-terminus seems to be also important for the stability of the protein, because with truncations larger than 70 amino acids we observed a decrease in the protein amount in cells (Figure 6d). Nevertheless, our results clearly show that the N-terminal hydrophilic extension preceding TMS1 is an important part of the protein involved in the regulation of *HsNHA2*'s function. Whether the structure of the conserved region between amino acids 45–60 or some posttranslational modification in this region are crucial for the regulation of *HsNHA2* is currently studied in our lab. Charged residues present in this segment could determine the flexibility of the N-terminus or they could be involved in intramolecular interactions and/or substrate attraction.

The core domain of Na^+/H^+ antiporters encapsulating the ion binding site includes two unwound transmembrane helices that cross each other in the middle of the membrane near the ion-binding site, creating an X-shaped structure, characteristic of the NhaA fold.⁴⁴ As for the membrane domain of *HsNHA2*, a comprehensive evolutionary analysis of 6,537 representative CPAs revealed a sequence motif of 8 amino acids residing on different transmembrane segments, but spatially close to each other around the substrate binding site.² In *HsNHA2*, this motif A243₁V244₂S245₃P246₄...₅...D278₆D279₇...R432₈ lacks the glutamate at position 5 present in other electrogenic CPA2 members. It was suggested that the electroneutrality of mammalian NHA2 is instead ensured by another glutamate (E215 in *HsNHA2*) in TMS 5 (Figures S1 and 8b) which forms a salt bridge with R432 at position 8 of the motif in TMS 12.² The glutamate residue located in TMS 5 (Figures 1 and S1) is unique in the *HsNHA2* and its homologs and cannot be found in other CPA2 members.² Cryo-EM structures of N-terminally truncated human (PDB 7B4M or 7B4L) or bison NHA2 confirmed the proximity of these two residues (Figure 8b; Protein Data Bank 7B4M or 7B4L²³). Our mutagenesis studies of full version of *HsNHA2* corroborate the results obtained for bison *NHA2* ΔN that, in

contrast to non-functional single-mutated versions (E215R or R432E), swapping up of E215 and R432 results in a Li^+ -selective transporter that transports Li^+ within the pH range 4.0–6.0 (Figure 4a,d). In addition, we show that the interaction between these two residues is also important for its structural integrity, and hence for the trafficking of the protein (Figure 4b,c).

Another residue that our study found to be highly important for the determination of *HsNHA2* transport properties is Pro246, located at position 4 in the conserved CPA motif close to the cation binding site D279 (Figure 8c). The presence of proline in any TMS perturbs the α -helical structure due to the flexibility of the ring structure of its side chain and the elimination of helix backbone hydrogen bonds for the carbonyls at positions i-3 and i-4.⁵⁴ In *HsNHA2*, Pro246 is located in TMS 6 (Figures 1 and S1), which is one of the two unwound transmembrane segments that create the X-shaped structure in CPAs' core domain (Figure 8c). Depending on the nature of the amino acid substituted at this position, we observed changes in the substrate specificity (ability to recognize and transport Li^+ or Na^+) of the antiporter (Figure 2a). Mutations of the corresponding proline residue to polar amino acids (Ser, Thr) in yeast Na^+/H^+ antiporters also resulted in altered substrate specificity toward larger cations.³⁷ In human NHE1, the replacement of this residue with alanine or glycine resulted in the loss of transport activity.^{55–57} In *Schizosaccharomyces pombe* sod2 antiporter, mutations of corresponding proline affected its structure and localization.⁵⁸ According to our results, the replacement of P246 with G, A, S or T did not change the targeting of *HsNHA2* to the plasma membrane or its stability (Figure 2b,c). Nevertheless, in particular the presence of the polar-branched threonine resulted in an antiporter that transports better Na^+ than Li^+ .

The cytosolic pH in growing *S. cerevisiae* cells is kept around a neutral value 7.0–7.2⁵⁹ and the activity of the native *HsNHA2* antiporter could only be detected at pH 4.0–5.5 (Figures 2a,e and 4a,d), that is, when there is a high gradient of protons across the plasma membrane. Interestingly, mutations P246S/T altered the pH dependent transport activity of *HsNHA2*, as it was highly active within the external pH range 4.0–7.4 (Figure 2a,e). Remarkably, measurements of Li^+ binding by the purified *E. coli* NhaA showed that a variant mutated at the corresponding residue at position 4 of the conserved CPA motif to threonine (I134T) also exhibited a decrease in pH dependence, but the affinity of this mutated version to Li^+ increased.⁶⁰ Similar to what was observed in *EcNhaA*, the altered pH-dependent activity of the P246 mutants could arise from the fact that this position is spatially close to the two aspartic acids in the antiporter's

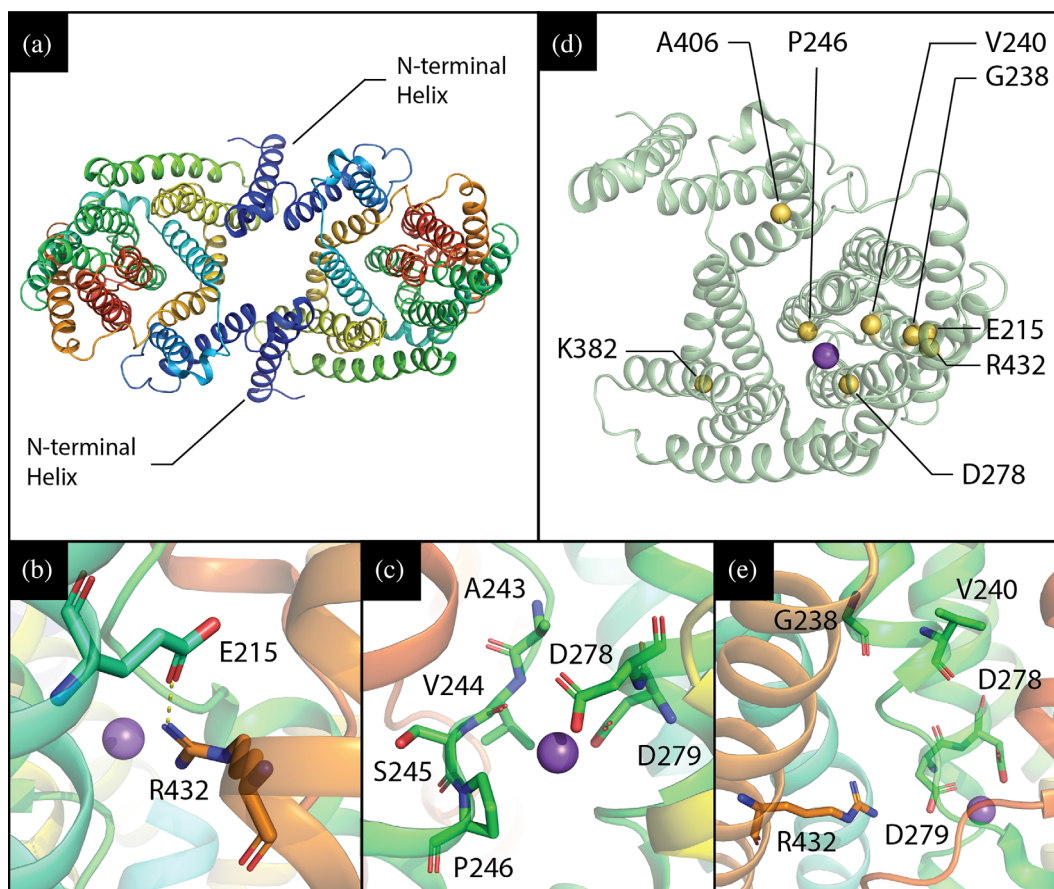


FIGURE 8 *HsNHA2* 3D-structure and location of various point mutations. (a) Structure of *HsNHA2* dimer, residues 79–521 (PDB entry 7B4L) in cartoon representation with rainbow coloring corresponding to N- through C-terminus. The additional N-terminal helix that is missing in other mammalian CPA members with known structures (dark blue) is highlighted. (b, c, e) Close-up view of studied *HsNHA2*'s point mutations in vicinity of ion-binding site. (b) Previously predicted E215-R432 salt bridge was recently confirmed by newly published structures of both human and bison NHA2, and is likely to play a structural role. (c) P246 is located at unwound section of TMS 6. Its surroundings are shown as sticks, and the bound sodium ion is shown as a purple sphere. Notably, the addition of a polar side-chain in the vicinity of D278 and D279, which mediate sodium and proton binding, could alter the pH-dependent activity of the antiporter. (e) G238, V240, D278 and R432, though they do not coordinate the sodium ion directly, are all located on the mobile and highly conserved core domain of the antiporter. (d) *HsNHA2* monomer, shown in cartoon representation, with position of various point mutations shown as yellow spheres. A sodium ion, observed in the experimental structure, is shown as a purple sphere and denotes the position of NHA2's binding site

binding site (D278 and D279). Specifically, the position equivalent to D279 was shown repeatedly to facilitate sodium binding and proton transport, apparently by alternating between a protonated and deprotonated state.^{2,31,61–63} It follows that the intrinsic pKa of this residue affects the antiporter's pH-dependent ion transport. D279's pKa shift in the P246 mutants can arise from two reasons. First, replacing the conformational-rigid proline with any other amino acid could alter the geometry of the highly conserved binding site. This could modify, for example, D279 hydration, thereby altering its pKa. Second, the most significant effect on NHA2's pH-dependent activity was observed for the P246T mutant. This implies that the addition of a polar residue like threonine in a

position that is spatially close to D279 could alter its pKa. Here we show *in vivo* that indeed mutations in position 246 can modulate cation and proton transport in *HsNHA2*.

Mutations of proline 246 to G, A, S or T provided the antiporter with highly increased resistance to the *HsNHA2*-specific inhibitor phloretin (Figure 3). It was found to efficiently inhibit for example, the enzymatic activity of tyrosinase⁶⁴ or glucose transporters GLUT,^{65,66} and thus it influences various physiological processes.^{67–69} Molecular docking showed that hydrophobic interaction and hydrogen bonding are the main non-covalent interaction forces between phloretin and tyrosinase.⁶⁴ So far, the molecular mechanism of the phloretin

inhibition of *HsNHA2* has not been studied. Here we show that the inhibition effect of phloretin did not change with mutations E215R + R432E in *HsNHA2*; however, it decreased significantly with alterations at the position of P246 (Figure 3). Thus, our results indicate that phloretin acts directly in the core domain of *HsNHA2* and mutations of P246 possibly cause inhibitor resistance by altering the binding site's geometry near the substrate/inhibitor-binding pocket, resulting from the substitution of the conformational-rigid proline with other amino acids. Figure 9 depicts a model of the bound phloretin to the native *HsNHA2* produced with Glid.^{70,71} Phloretin is predicted to directly interact with D279 in *HsNHA2*'s binding site.

There are significant differences between the genomes of human individuals due to single-nucleotide variants (polymorphisms, SNPs). In this study, we characterized the effect of six mutations existing as SNPs in human *NHA2*³⁹ on the antiporter's transport activity, substrate specificity and localization (Figure 5). The positions of mutated residues within the *HsNHA2* monomer in relation to the cation-binding site are shown in Figure 8d. Residues G238, V240, D278 and R432, though they do not coordinate the transported cation (Na^+ or Li^+) directly, are all located on the mobile and highly conserved core domain of the antiporter (Figure 8e). Our data show that this *in vivo* experimental approach can be highly useful for a rapid screening of SNP's effect on *HsNHA2* activity. Here, it enabled us to distinguish the various effects of mutations on *HsNHA2* properties at the molecular level (e.g., effect on substrate specificity—R432Q; transport mechanism—D278G or protein folding and trafficking—G238R; Figure 5). A more detail quantification of the total amount of proteins in cells with the estimation of their amount in the plasma membrane would bring even more knowledge on the effect of particular SNP(s) on the structure, stability and plasma-membrane targeting of *HsNHA2*.

Remarkably, the K382E mutation was found to be associated with hypertension.³⁹ Positively charged residues are more abundant in the cytoplasmic side of many membrane proteins (“positive-inside rule”) and the substitution of such residue with an opposite charge could potentially affect the proper insertion and orientation of the protein to the membrane.^{72–74} Notably, the positively charged K382 is located far from the cation-binding site, facing the cytoplasm (Figure 8d), its replacement with negatively charged glutamate did not change the plasma-membrane localization of the antiporter (Figure 5b), but it resulted in restricted substrate specificity for Li^+ alone and very low transport activity (ability to improve the LiCl tolerance of cells) (Figure 5a). On the other hand, the V240L mutation in the antiporter's core domain (Figure 8d,e) had only minor effect on *HsNHA2*'s

functionality (Figure 5), probably, due to its conservative nature. Furthermore, these results are in line with V240 positioning roughly 12 Å away from where the sodium ion binds (based on the Na^+ -bound structure of the *HsNHA2*; PDB entry 7B4L; Figure 8d). Thus, the combination of our experimental expression model for *HsNHA2* with molecular modeling can be used to characterize various pathology-related SNPs that exist in the *HsNHA2* gene in the future.

4 | CONCLUSION

In general, our work provides new and important knowledge on using *S. cerevisiae* as a host for studying human membrane transporters. Specifically, it provides new valuable knowledge on the structure and function of the human Na^+/H^+ antiporter *NHA2* that has broad physiological functions in the human body, and whose mal-functioning results in a growing list of pathologies. We identified several amino-acid residues important for *HsNHA2* substrate specificity, transport activity, stability and trafficking that had not been characterized previously. Furthermore, our optimized expression system of *HsNHA2* in yeast cells may be a powerful tool for the efficient screening of compounds that can activate/inhibit *HsNHA2* activity, for the selection of other inhibitor-resistant mutants to elucidate structure-activity relationships, or for discovering the molecular mechanism of inhibitors' actions in *HsNHA2*. Newly identified mutated versions of *HsNHA2* with higher activity and higher resistance to phloretin than the native antiporter may also serve as controls in future *HsNHA2* studies. Moreover, our findings concerning a unique regulatory/autoinhibitory role of the hydrophilic N-terminal part of the protein will definitely be useful for future studies of *NHA2* regulation in human cells.

5 | MATERIALS AND METHODS

5.1 | Yeast strains and growth media

Alkali-metal-cation-sensitive *S. cerevisiae* W303-1A derivatives—BW31 (*ena1Δ::HIS3::ena4Δ nha1Δ::LEU2*)³⁷ or AB11c (*ena1Δ::HIS3::ena4Δ nha1Δ::LEU2 nhx1Δ::TRP1*)⁷⁵ lacking genes encoding plasma-membrane *Ena* ATPases, plasma-membrane antiporter *Nha1* or intracellular antiporter *Nhx1* were used to characterize *HsNHA2* activity *in vivo*. Yeast cultures were routinely grown in YPD (Formedium, Hunstanton, UK) or YNB media (Difco, Sparks, MD) at 30°C. YNB-based media (referred in this work as YNB-Pro) contained 0.17% YNB without

amino acids and ammonium sulfate, 0.1% proline, and 2 or 4% glucose. Proline was used instead of ammonium sulfate as a nitrogen source. A mixture of appropriate auxotrophic supplements (adenine, tryptophan, leucine, and histidine—each at a final concentration of 20 or 40 $\mu\text{g}/\text{ml}$) was added after autoclaving. YPD media were supplemented with extra adenine (final concentration 20 $\mu\text{g}/\text{ml}$) to avoid additional spontaneous mutagenesis caused by the *ade2* mutation present in both strains. Solid media were prepared by adding 2 or 3% (w/v) agar.

5.2 | Plasmids

The plasmids used in this study are listed in Table 1. All new plasmids were constructed by homologous recombination in the *S. cerevisiae* BW31 strain by using a series of overlapping PCR products and a linearized plasmid (pNHA1-985, pENA1, or pENA1-GFP; Table 1), in which the original gene was replaced by the corresponding *HsNHA2* cDNA or its appropriately truncated versions. The oligonucleotides used for PCR and the construction of particular plasmids are listed in Table S1. *HsNHA2* cDNA encoding full or N-terminally truncated versions of the antiporter were amplified from pTEF1-*HsNHA2*-HA (Table 1). The sequence corresponding to GFP or the *ScTPS1* terminator were amplified from pGRU1 or YEp352-ZrSTL1-TPS1t-kanMX, respectively (Table 1). In all new plasmids, the expression of *HsNHA2* variants was under the control of the weak and constitutive *S. cerevisiae* *NHA1* promoter.²⁰ The resulting plasmids were based on multicopy vectors YEp352 or pGRU1 (Table 1). Plasmids containing N-terminally GFP-tagged versions of *HsNHA2* (native or truncated) were constructed by inserting a GFP-encoding sequence in frame at the 5'-end. In p*HsNHA2*-GFP, the GFP was added in frame at the 3'-end in front of the STOP codon. In p*HsNHA2t* and pGFP-*HsNHA2t* plasmids, the *ScTPS1* terminator was inserted behind the *HsNHA2* cDNA. To generate centromeric versions of p*HsNHA2t* and pGFP-*HsNHA2t*, the 2 μ sequence was replaced by homologous recombination with the sequence corresponding to a centromere amplified from pRS316,²¹ and the resulting plasmids were named pC-*HsNHA2t* and pC-GFP-*HsNHA2t* (Table 1). *Escherichia coli* XL1-Blue (Agilent Technologies, Santa Clara, CA) was used for pDNA amplification. Successful cloning was verified by restriction analysis and sequencing.

Point mutations were introduced into p*HsNHA2t* or pGFP-p*HsNHA2t* using a QuikChange XL Site-Directed Mutagenesis kit (Agilent Technologies) and the corresponding oligonucleotides (Table S1). The accuracy of mutations was confirmed by sequencing.

5.3 | Growth assays

To estimate the cell tolerance to different alkali-metal cations, YNB-Pro media were supplemented with LiCl, NaCl or KCl at the indicated concentration. HCl or TEA (triethylamine) were used to adjust the pH. Media with buffered pH were supplemented either with 20 mM MES (pH 5.5 and pH 6.0) or 20 mM MOPS (pH 7.0 and pH 7.4), and the required pH was adjusted as above. To test the activity inhibition of *HsNHA2* and its variants, media were supplemented with a solution of phloretin (Merck, Darmstadt, Germany; cat. no. P7912) dissolved in DMSO (100 mM stock solution). Tenfold serial dilutions of fresh cell suspensions ($\text{OD}_{600} = 2$, Eppendorf BioPhotometer, Hamburg, Germany) were spotted on plates as indicated, and growth was monitored for 2–10 days. Representative results of at least three independent experiments are shown.

5.4 | Fluorescence microscopy

Microscopic images of yeast cells were acquired with an Olympus BX53 microscope with an Olympus DP73 camera (Olympus, Tokio, Japan). A Cool LED light source with 460 nm excitation and 515 nm emission was used to visualize *HsNHA2* and its variants or *ScNha1* tagged with GFP (expressed from plasmids pGFP-*HsNHA2t*, p*HsNHA2*-GFP or pNHA1-985GFP, respectively, Table 1). Cells containing the corresponding multi-copy plasmids were grown overnight in YNB-Pro with 4% glucose and supplemented with adenine and tryptophan (final concentration 40 $\mu\text{g}/\text{ml}$), and leucine and histidine (final concentration 20 $\mu\text{g}/\text{ml}$). Cells were observed when they reached the exponential phase ($\text{OD}_{600} \approx 0.3\text{--}0.5$). A Nomarski prism was used for whole-cell images.

5.5 | Cation loss determination

Sodium efflux was determined similarly as previously described.³⁷ Cells were grown in YNB-Pro medium to the early exponential phase ($\text{OD}_{600} \approx 0.2\text{--}0.3$, Spekol, Carl Zeiss, Oberkochen, Germany), harvested, resuspended, and incubated in YNB-Pro supplemented with 100 mM NaCl at pH 7.0 (to preload them with sodium) for 60 min at 30°C. Cells were collected by centrifugation, washed with deionized water, and resuspended in an incubation buffer (10 mM Tris, 0.1 mM MgCl_2 , 2% glucose). The pH of the buffer was first brought down to 3.9 with citric acid and then adjusted to 4.0 with $\text{Ca}(\text{OH})_2$. The buffer was supplemented with 10 mM KCl to prevent Na^+ reuptake. Samples of cell suspensions were withdrawn at intervals

over 90 min. Cells were harvested by filtration (Millipore membrane filters, Merck-Millipore, Cork, Ireland), washed with 20 mM MgCl₂, acid extracted, and the cation content in samples was determined by atomic absorption spectrometry.³⁷ Data obtained in at least three independent experiments are shown as the average amount of sodium lost from cells over 90 min \pm SD.

5.6 | Protein extraction and immunoblotting

Yeast cells containing the pGFP-*HsNHA2t* plasmid or its variants were grown in liquid YNB-Pro media to the exponential phase (OD₆₀₀ \approx 0.6–0.8, Spekol, Carl Zeiss), collected by centrifugation, and washed once with deionized cold water. Cell pellets were kept at -80°C . Total extracts of proteins from cells were then prepared as described previously.⁷⁶ The RCDC protein assay (Bio-Rad, Hercules, CA) was used for the quantification of proteins. Samples of total protein extracts (120 μg per sample) were separated by 10% SDS-PAGE and transferred to nitrocellulose membranes (Trans-Blot Turbo 0.2 μm nitrocellulose, Bio-Rad) using a Trans-Blot Turbo Transfer System (Bio-Rad). Membranes were incubated overnight at 4°C with an anti-GFP monoclonal antibody (Roche, Basel, Switzerland; dilution 1:500), washed and then incubated with a secondary anti-mouse IgG

antibody tagged with a horseradish peroxidase (GE Healthcare, Chicago, IL; dilution 1:10,000). Immunoreactive proteins were visualized with a Clarity Max Western ECL substrate kit (Bio-Rad) in ChemiDoc visualizer (Bio-Rad). To detect Pgk1 protein (as a protein loading control), the same membranes used for GFP-*HsNHA2* were reprobated after being incubated with an anti-Pgk1 mouse monoclonal antibody (Abcam, Cambridge, UK; dilution 1:20,000) for 1 hr at room temperature, incubated with the secondary antibody, and detected as above.

5.7 | *HsNHA2* evolutionary conservation analysis

The conservation analysis for *HsNHA2*'s N-terminus was conducted using the ConSurf web server.⁷⁷ A total of 99 unique sequences were collected by HMMER from the UniRef90 database with sequence identity ranging between 35 and 95% and an *E*-value lower than 10^{-5} .

5.8 | Modeling of phloretin binding to *HsNHA2*

A molecule of phloretin was docked to the crystal structure of human NHA2 (PDB entry 7B4L) using Glide.⁷⁰

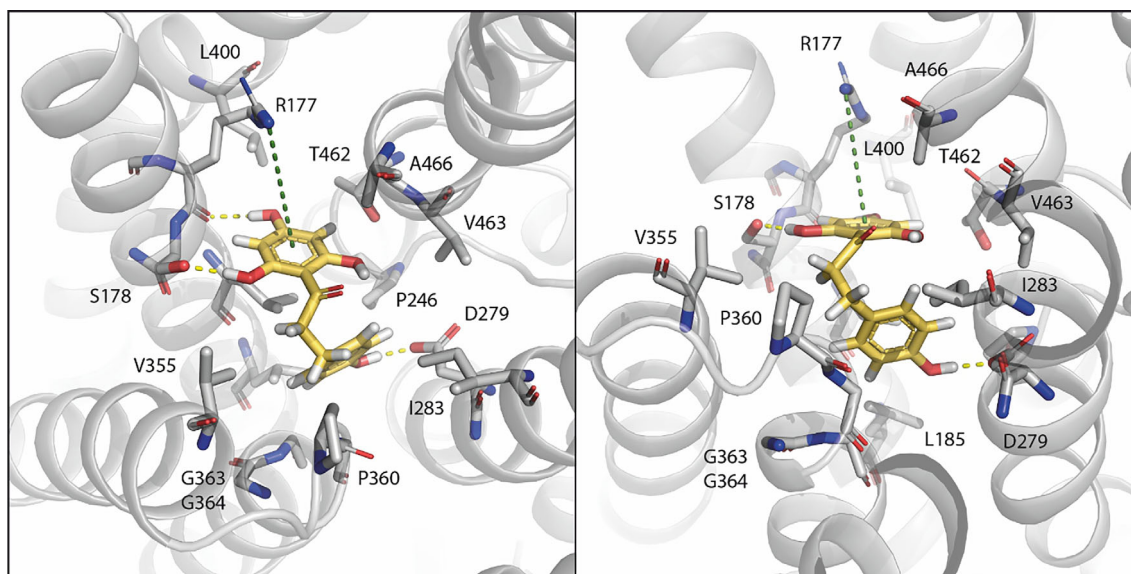


FIGURE 9 A model of phloretin binding to *HsNHA2*. Phloretin, shown in yellow, was docked to the crystal structure of human NHA2 (PDB entry 7B4L) as described in Material and Methods and is shown in two different views. Residues within a radius of 5 Å from phloretin are shown as sticks. Phloretin is stabilized by three amino acids. The 2,4,6-trihydroxyphenyl ring interacts via hydrogen bonds with the side chain hydroxyl of S178 and the backbone carbonyl of R177. It also forms cation- π interaction with the side chain guanidinium of R177. The 4-hydroxyphenyl ring hydrogen bonds with the highly conserved D279 in *HsNHA2* binding site, that facilitates both proton and cation transport

The crystal structure was initially prepared for docking using the Protein Preparation Wizard.⁷⁸ The protonation states of all residues were determined with PROPKA3,⁷⁹ with an exception of D278 and D279, which were modeled in all combinations of protonation states. In Figure 9, we arbitrarily show both D278 and D279 in their deprotonated state. The docking poses were scored and selected according to the extra precision scoring function (XP).⁷¹ The docking score for the *HsNHA2*-phloretin complex ranges from -4.9 to -6.4 kcal/mol depending on the different protonation states of D278 and D279. It should be noted that despite their energy units, docking scores are not equivalent to real world ΔG values, as they are calculated based on a single conformation of the ligand-protein complex and neglect dynamic and entropic contributions associated with the small molecule binding. The figure was produced using PyMOL (The PyMOL Molecular Graphics System, Version 2.5, Schrödinger).

5.9 | Statistics

Data presented are either from a representative experiment or from the mean of replicative values plus or minus standard deviation. Statistically significant differences were analysed by unpaired Student *t*-test using Microsoft Office Excel 2016 (** $p < .01$).

AUTHOR CONTRIBUTIONS

Diego Velázquez: Conceptualization (equal); data curation (equal); investigation (lead); visualization (equal); writing – original draft (equal); writing – review and editing (supporting). **Vojtěch Průša:** Investigation (supporting). **Gal Masrati:** Data curation (supporting); investigation (supporting); visualization (supporting); writing – review and editing (supporting). **Elon Yariv:** Investigation (supporting). **Hana Sychrova:** Supervision (supporting); writing – review and editing (supporting). **Nir Ben-Tal:** Data curation (supporting); funding acquisition (supporting); supervision (equal); writing – review and editing (equal). **Olga Zimmermannova:** Conceptualization (lead); data curation (equal); formal analysis (lead); funding acquisition (lead); investigation (supporting); methodology (lead); project administration (lead); supervision (lead); validation (lead); writing – original draft (lead); writing – review and editing (lead).

ACKNOWLEDGMENTS

The technical assistance of Pavla Herynková is highly acknowledged. We thank Daniel Fuster, MD, for providing us the plasmid pTEF1-*HsNHA2*-HA. We wish to thank Dr. Raghu Metpally and Prof. Rajini Rao for

providing information about mutations identified as SNPs in *HsNHA2* that we characterized in this study. Prof. Rajini Rao and Prof. Pierre Falson are highly acknowledged also for a stimulating and fruitful discussion.

FUNDING INFORMATION

The work of Olga Zimmermannova group was supported by a GAČR grant 21-08985S. The work of Diego Velázquez was supported by IPHYS Mobility II, CZ.02.2.69/0.0/0.0/18_053/0016977. The work of Nir Ben-Tal group was supported by Grant 2017293 of the USA–Israel Binational Science Foundation and the Abraham E. Kazan Chair in Structural Biology, Tel Aviv University.

CONFLICT OF INTEREST

The authors declare no conflict of interest.

DATA AVAILABILITY STATEMENT

The data that support the findings of this study are available from the corresponding author upon reasonable request.

ORCID

Diego Velázquez  <https://orcid.org/0000-0002-5987-2570>
 Gal Masrati  <https://orcid.org/0000-0003-1322-5762>
 Elon Yariv  <https://orcid.org/0000-0001-7457-2608>
 Hana Sychrova  <https://orcid.org/0000-0001-5967-5019>
 Nir Ben-Tal  <https://orcid.org/0000-0001-6901-832X>
 Olga Zimmermannova  <https://orcid.org/0000-0003-2538-4488>

REFERENCES

1. Padan E, Landau M. Sodium-proton Na^+/H^+ antiporters: Properties and roles in health and disease. *Metal Ions Life Sci*. 2016; 16:391–458. https://doi.org/10.1007/978-3-319-21756-7_12.
2. Masrati G, Dwivedi M, Rimon A, et al. Broad phylogenetic analysis of cation/proton antiporters reveals transport determinants. *Nat Commun*. 2018;9:4205. <https://doi.org/10.1038/s41467-018-06770-5>.
3. Pedersen SF, Counillon L. The SLC9A-C mammalian Na^+/H^+ exchanger family: Molecules, mechanisms, and physiology. *Physiol Rev*. 2019;99:2015–2113. <https://doi.org/10.1152/physrev.00028.2018>.
4. Fuster DG, Zhang J, Shi M, Bobulescu IA, Andersson S, Moe OW. Characterization of the sodium/hydrogen exchanger NHA2. *J Am Soc Nephrol*. 2008;19:1547–1556. <https://doi.org/10.1681/ASN.2007111245>.
5. Battaglino RA, Pham L, Morse LR, et al. NHA-oc/NHA2: A mitochondrial cation-proton antiporter selectively expressed in osteoclasts. *Bone*. 2008;42:180–192. <https://doi.org/10.1016/j.bone.2007.09.046>.
6. Xiang M, Feng M, Muend S, Rao R. A human Na^+/H^+ antiporter sharing evolutionary origins with bacterial NhaA may be a

- candidate gene for essential hypertension. *Proc Natl Acad Sci U S A.* 2007;104:18677–18681. <https://doi.org/10.1073/pnas.0707120104>.
7. Chintapalli VR, Kato A, Henderson L, et al. Transport proteins NHA1 and NHA2 are essential for survival, but have distinct transport modalities. *Proc Natl Acad Sci U S A.* 2015;112:11720–11725. <https://doi.org/10.1073/pnas.1508031112>.
 8. Deisl C, Simonin A, Anderegg M, et al. Sodium/hydrogen exchanger NHA2 is critical for insulin secretion in beta-cells. *Proc Natl Acad Sci U S A.* 2013;110:10004–10009. <https://doi.org/10.1073/pnas.1220009110>.
 9. Deisl C, Anderegg M, Albano G, et al. Loss of sodium/hydrogen exchanger NHA2 exacerbates obesity- and aging-induced glucose intolerance in mice. *PLoS One.* 2016;11:e0163568. <https://doi.org/10.1371/journal.pone.0163568>.
 10. Liu HM, He JY, Zhang Q, et al. Improved detection of genetic loci in estimated glomerular filtration rate and type 2 diabetes using a pleiotropic cFDR method. *Mol Genet Genomics.* 2018;293:225–235. <https://doi.org/10.1007/s00438-017-1381-6>.
 11. Kondapalli KC, Todd Alexander R, Pluznick JL, Rao R. NHA2 is expressed in distal nephron and regulated by dietary sodium. *J Physiol Biochem.* 2017;73:199–205. <https://doi.org/10.1007/s13105-016-0539-8>.
 12. Anderegg MA, Albano G, Hanke D, et al. The sodium/proton exchanger NHA2 regulates blood pressure through a WNK4-NCC dependent pathway in the kidney. *Kidney Int.* 2021;99:350–363. <https://doi.org/10.1016/j.kint.2020.08.023>.
 13. Prasad H, Dang DK, Kondapalli KC, Natarajan N, Cebotaru V, Rao R. NHA2 promotes cyst development in an in vitro model of polycystic kidney disease. *J Physiol.* 2019;597:499–519. <https://doi.org/10.1113/JP276796>.
 14. Chen SR, Chen M, Deng SL, Hao XX, Wang XX, Liu YX. Sodium-hydrogen exchanger NHA1 and NHA2 control sperm motility and male fertility. *Cell Death Dis.* 2016;7:e2152. <https://doi.org/10.1038/cddis.2016.65>.
 15. Ha BG, Hong JM, Park JY, et al. Proteomic profile of osteoclast membrane proteins: Identification of Na⁺/H⁺ exchanger domain containing 2 and its role in osteoclast fusion. *Proteomics.* 2008;8:2625–2639. <https://doi.org/10.1002/pmic.200701192>.
 16. Lee SH, Kim T, Park ES, et al. NHE10, an osteoclast-specific member of the Na⁺/H⁺ exchanger family, regulates osteoclast differentiation and survival [corrected]. *Biochem Biophys Res Commun.* 2008;369:320–326. <https://doi.org/10.1016/j.bbrc.2008.01.168>.
 17. Hofstetter W, Siegrist M, Simonin A, Bonny O, Fuster DG. Sodium/hydrogen exchanger NHA2 in osteoclasts: Subcellular localization and role in vitro and in vivo. *Bone.* 2010;47:331–340. <https://doi.org/10.1016/j.bone.2010.04.605>.
 18. Charles JF, Coury F, Sulyanto R, et al. The collection of NFATc1-dependent transcripts in the osteoclast includes numerous genes non-essential to physiologic bone resorption. *Bone.* 2012;51:902–912. <https://doi.org/10.1016/j.bone.2012.08.113>.
 19. Hill JE, Myers AM, Koerner TJ, Tzagoloff A. Yeast/*E. coli* shuttle vectors with multiple unique restriction sites. *Yeast.* 1986;2:163–167. <https://doi.org/10.1002/yea.320020304>.
 20. Kinclova O, Ramos J, Potier S, Sychrova H. Functional study of the *Saccharomyces cerevisiae* Nha1p C-terminus. *Mol Microbiol.* 2001;40:656–668. <https://doi.org/10.1046/j.1365-2958.2001.02412.x>.
 21. Sikorski RS, Hieter P. A system of shuttle vectors and yeast host strains designed for efficient manipulation of DNA in *Saccharomyces cerevisiae*. *Genetics.* 1989;122:19–27. <https://doi.org/10.1093/genetics/122.1.19>.
 22. Duskova M, Ferreira C, Lucas C, Sychrova H. Two glycerol uptake systems contribute to the high osmotolerance of *Zygosaccharomyces rouxii*. *Mol Microbiol.* 2015;97:541–559. <https://doi.org/10.1111/mmi.13048>.
 23. Matsuoka R, Fudim R, Jung S, et al. Structure, mechanism and lipid-mediated remodeling of the mammalian Na⁺/H⁺ exchanger NHA2. *Nat Struct Mol Biol.* 2022;29:108–120. <https://doi.org/10.1038/s41594-022-00738-2>.
 24. Varadi M, Anyango S, Deshpande M, et al. AlphaFold protein structure database: Massively expanding the structural coverage of protein-sequence space with high-accuracy models. *Nucleic Acids Res.* 2022;50:D439–D444. <https://doi.org/10.1093/nar/gkab1061>.
 25. Hendus-Altenburger R, Kragelund BB, Pedersen SF. Structural dynamics and regulation of the mammalian SLC9A family of Na⁺/H⁺ exchangers. *Curr Top Membr.* 2014;73:69–148. <https://doi.org/10.1016/B978-0-12-800223-0.00002-5>.
 26. Chow CW, Woodside M, Demaurex N, et al. Proline-rich motifs of the Na⁺/H⁺ exchanger 2 isoform-binding of Src homology domain 3 and role in apical targeting in epithelia. *J Biol Chem.* 1999;274:10481–10488. <https://doi.org/10.1074/jbc.274.15.10481>.
 27. Onishi I, Lin PJ, Diering GH, Williams WP, Numata M. Rack1 associates with NHE5 in focal adhesions and positively regulates the transporter activity. *Cell Signal.* 2007;19:194–203. <https://doi.org/10.1016/j.cellsig.2006.06.011>.
 28. Fukura N, Ohgaki R, Matsushita M, Nakamura N, Mitsui K, Kanazawa H. A membrane-proximal region in the C-terminal tail of NHE7 is required for its distribution in the trans-Golgi network, distinct from NHE6 localization at endosomes. *J Membr Biol.* 2010;234:149–158. <https://doi.org/10.1007/s00232-010-9242-9>.
 29. Uzdavinyus P, Coinçon M, Nji E, et al. Dissecting the proton transport pathway in electrogenic Na⁺/H⁺ antiporters. *Proc Natl Acad Sci U S A.* 2017;114:E1101–E1110. <https://doi.org/10.1073/pnas.1614521114>.
 30. Kondapalli KC, Kallay LM, Muszelik M, Rao R. Unconventional chemiosmotic coupling of NHA2, a mammalian Na⁺/H⁺ antiporter, to a plasma membrane H⁺ gradient. *J Biol Chem.* 2012;287:36239–36250. <https://doi.org/10.1074/jbc.M112.403550>.
 31. Schushan M, Xiang M, Bogomiakov P, Padan E, Rao R, Ben-Tal N. Model-guided mutagenesis drives functional studies of human NHA2, implicated in hypertension. *J Mol Biol.* 2010;396:1181–1196. <https://doi.org/10.1016/j.jmb.2009.12.055>.
 32. Flegelova H, Haguenaer-Tsapis R, Sychrova H. Heterologous expression of mammalian Na⁺/H⁺ antiporters in *Saccharomyces cerevisiae*. *Biochim Biophys Acta.* 2006;1760:504–516. <https://doi.org/10.1016/j.bbagen.2006.01.014>.
 33. Flegelova H, Sychrova H. Mammalian NHE2 Na⁺/H⁺ exchanger mediates efflux of potassium upon heterologous expression in yeast. *FEBS Lett.* 2005;579:4733–4738. <https://doi.org/10.1016/j.febslet.2005.07.046>.

34. Banuelos MA, Ruiz MC, Jiménez A, Souciet JL, Potier S, Ramos J. Role of the Nha1 antiporter in regulating K⁺ influx in *Saccharomyces cerevisiae*. *Yeast*. 2002;19:9–15. <https://doi.org/10.1002/yea.799>.
35. Zhao J, Hyman L, Moore C. Formation of mRNA 3' ends in eukaryotes: Mechanism, regulation, and interrelationships with other steps in mRNA synthesis. *Microbiol Mol Biol Rev*. 1999;63:405–445. <https://doi.org/10.1128/MMBR.63.2.405-445.1999>.
36. Yamanishi M, Katahira S, Matsuyama T. *TPS1* terminator increases mRNA and protein yield in a *Saccharomyces cerevisiae* expression system. *Biosci Biotechnol Biochem*. 2011;75:2234–2236. <https://doi.org/10.1271/bbb.110246>.
37. Kinclova-Zimmermannova O, Zavrel M, Sychrova H. Identification of conserved prolyl residue important for transport activity and the substrate specificity range of yeast plasma membrane Na⁺/H⁺ antiporters. *J Biol Chem*. 2005;280:30638–30647. <https://doi.org/10.1074/jbc.M506341200>.
38. Behzad S, Sureda A, Barreca D, Nabavi SF, Rastrelli L, Nabavi SM. Health effects of phloretin: From chemistry to medicine. *Phytochem Rev*. 2017;16:527–533. <https://doi.org/10.1007/s11101-017-9500-x>.
39. Dewey FE, Murray MF, Overton JD, et al. Distribution and clinical impact of functional variants in 50,726 whole-exome sequences from the discover study. *Science*. 2016;354:aaf6814. <https://doi.org/10.1126/science.aaf6814>.
40. Su P, Wu H, Wang M, Cai L, Liu Y, Chen LM. Irbit activates NBCe1-B by releasing the auto-inhibition module from the transmembrane domain. *J Physiol*. 2021;599:1151–1172. <https://doi.org/10.1113/JP280578>.
41. Thines L, Deschamps A, Stribny J, Morsomme P. Yeast as a tool for deeper understanding of human manganese-related diseases. *Genes (Basel)*. 2019;10:545. <https://doi.org/10.3390/genes10070545>
42. Stribny J, Thines L, Deschamps A, Goffin P, Morsomme P. The human Golgi protein TMEM165 transports calcium and manganese in yeast and bacterial cells. *J Biol Chem*. 2020;295:3865–3874. <https://doi.org/10.1074/jbc.RA119.012249>.
43. Hunte C, Screpanti E, Venturi M, Rimon A, Padan E, Michel H. Structure of a Na⁺/H⁺ antiporter and insights into mechanism of action and regulation by pH. *Nature*. 2005;435:1197–1202. <https://doi.org/10.1038/nature03692>.
44. Padan E. Functional and structural dynamics of NhaA, a prototype for Na⁺ and H⁺ antiporters, which are responsible for Na⁺ and H⁺ homeostasis in cells. *Biochim Biophys Acta*. 2014;1837:1047–1062. <https://doi.org/10.1016/j.bbabi.2013.12.007>.
45. Dong Y, Gao Y, Ilie A, et al. Structure and mechanism of the human NHE1-CHP1 complex. *Nat Commun*. 2021;12:3474. <https://doi.org/10.1038/s41467-021-23496-z>.
46. Winklemann I, Matsuoka R, Meier PF, et al. Structure and elevator mechanism of the mammalian sodium/proton exchanger NHE9. *EMBO J*. 2020;39:e105908. <https://doi.org/10.15252/embj.2020105908>.
47. Lee C, Kang HJ, Von Ballmoos C, et al. A two-domain elevator mechanism for sodium/proton antiport. *Nature*. 2013;501:573–577. <https://doi.org/10.1038/nature12484>.
48. Paulino C, Wohlert D, Kapotova E, Yildiz O, Kuhlbrandt W. Structure and transport mechanism of the sodium/proton antiporter MjNhaP1. *eLife*. 2014;3:e03583. <https://doi.org/10.7554/eLife.03583>.
49. Wohlert D, Kuhlbrandt W, Yildiz O. Structure and substrate ion binding in the sodium/proton antiporter PaNhaP. *eLife*. 2014;3:e03579. <https://doi.org/10.7554/eLife.03579>.
50. Goswami P, Paulino C, Hizlan D, Vonck J, Yildiz Ö, Kuhlbrandt W. Structure of the archaeal Na⁺/H⁺ antiporter NhaP1 and functional role of transmembrane helix 1. *EMBO J*. 2011;30:439–449. <https://doi.org/10.1038/emboj.2010.321>.
51. Smidova A, Stankova K, Petrvalska O, et al. The activity of *Saccharomyces cerevisiae* Na⁺, K⁺/H⁺ antiporter Nha1 is negatively regulated by 14-3-3 protein binding at serine 481. *Biochim Biophys Acta Mol Cell Res*. 2019;1866:118534. <https://doi.org/10.1016/j.bbamcr.2019.118534>.
52. Pittman JK, Sreevidya CS, Shigaki T, Ueoka-Nakanishi H, Hirschi KD. Distinct N-terminal regulatory domains of Ca²⁺/H⁺ antiporters. *Plant Physiol*. 2002;130:1054–1062. <https://doi.org/10.1104/pp.008193>.
53. Cagnac O, Baghour M, Jaime-Pérez N, et al. Deletion of the N-terminal domain of the yeast vacuolar Na⁺, K⁺/H⁺ antiporter Vnx1p improves salt tolerance in yeast and transgenic arabidopsis. *Yeast*. 2020;37:173–185. <https://doi.org/10.1002/yea.3450>.
54. Visiers I, Braunheim BB, Weinstein H. Prokink: A protocol for numerical evaluation of helix distortions by proline. *Protein Eng*. 2000;13:603–606. <https://doi.org/10.1093/protein/13.9.603>.
55. Counillon L, Noel J, Reithmeier RA, Pouyssegur J. Random mutagenesis reveals a novel site involved in inhibitor interaction within the fourth transmembrane segment of the Na⁺/H⁺ exchanger-1. *Biochemistry*. 1997;36:2951–2959. <https://doi.org/10.1021/bi9615405>.
56. Slepkov ER, Rainey JK, Li X, et al. Structural and functional characterization of transmembrane segment IV of the NHE1 isoform of the Na⁺/H⁺ exchanger. *J Biol Chem*. 2005;280:17863–17872. <https://doi.org/10.1074/jbc.M409608200>.
57. Slepkov ER, Chow S, Lemieux MJ, Fliegel L. Proline residues in transmembrane segment IV are critical for activity, expression and targeting of the Na⁺/H⁺ exchanger isoform 1. *Biochem J*. 2004;379:31–38. <https://doi.org/10.1042/BJ20030884>.
58. Ndayizeye M, Touret N, Fliegel L. Proline 146 is critical to the structure, function and targeting of sod2, the Na⁺/H⁺ exchanger of *Schizosaccharomyces pombe*. *Biochim Biophys Acta*. 2009;1788:983–992. <https://doi.org/10.1016/j.bbamem.2009.01.001>.
59. Zimmermannova O, Felcmanová K, Rosas-Santiago P, Papoušková K, Pantoja O, Sychrová H. Erv14 cargo receptor participates in regulation of plasma-membrane potential, intracellular pH and potassium homeostasis via its interaction with K⁺-specific transporters Trk1 and Tok1. *BBA-Mol Cell Res*. 2019;1866:1376–1388. <https://doi.org/10.1016/j.bbamcr.2019.05.005>.
60. Mondal R, Rimon A, Masrati G, Ben-Tal N, Friedler A, Padan E. Towards molecular understanding of the pH dependence characterizing NhaA of which structural fold is shared by other transporters. *J Mol Biol*. 2021;433:167156. <https://doi.org/10.1016/j.jmb.2021.167156>.
61. Furrer EM, Ronchetti MF, Verrey F, Pos KM. Functional characterization of a NapA Na⁺/H⁺ antiporter from *Thermus thermophilus*. *FEBS Lett*. 2007;581:572–578. <https://doi.org/10.1016/j.febslet.2006.12.059>.
62. Inoue H, Noumi T, Tsuchiya T, Kanazawa H. Essential aspartic acid residues, Asp-133, Asp-163 and Asp-164, in the transmembrane helices of a Na⁺/H⁺ antiporter (NhaA) from *Escherichia*

- coli*. FEBS Lett. 1995;363:264–268. [https://doi.org/10.1016/0014-5793\(95\)00331-3](https://doi.org/10.1016/0014-5793(95)00331-3).
63. Kuwabara N, Inoue H, Tsuboi Y, Mitsui K, Matsushita M, Kanazawa H. Structure-function relationship of the fifth transmembrane domain in the Na⁺/H⁺ antiporter of *Helicobacter pylori*: Topology and function of the residues, including two consecutive essential aspartate residues. *Biochemistry*. 2006;45:14834–14842. <https://doi.org/10.1021/bi061048d>.
64. Chen J, Li Q, Ye Y, Huang Z, Ruan Z, Jin N. Phloretin as both a substrate and inhibitor of tyrosinase: Inhibitory activity and mechanism. *Spectrochim Acta A Mol Biomol Spectrosc*. 2020;226:117642. <https://doi.org/10.1016/j.saa.2019.117642>.
65. Lin ST, Tu SH, Yang PS, et al. Apple polyphenol phloretin inhibits colorectal cancer cell growth via inhibition of the type 2 glucose transporter and activation of p53-mediated signaling. *J Agric Food Chem*. 2016;64:6826–6837. <https://doi.org/10.1021/acs.jafc.6b02861>.
66. Liu L, Xie H, Zhao S, Huang X. The GLUT1-mtORC1 axis affects odontogenic differentiation of human dental pulp stem cells. *Tissue Cell*. 2022;76:101766. <https://doi.org/10.1016/j.tice.2022.101766>.
67. Casado-Díaz A, Rodríguez-Ramos Á, Torrecillas-Baena B, Dorado G, Quesada-Gómez JM, Gálvez-Moreno MÁ. Flavonoid phloretin inhibits adipogenesis and increases OPG expression in adipocytes derived from human bone-marrow mesenchymal stromal-cells. *Nutrients*. 2021;13:4185. <https://doi.org/10.3390/nu13114185>.
68. Wu KH, Ho CT, Chen ZF, et al. The apple polyphenol phloretin inhibits breast cancer cell migration and proliferation via inhibition of signals by type 2 glucose transporter. *J Food Drug Anal*. 2018;26:221–231. <https://doi.org/10.1016/j.jfda.2017.03.009>.
69. Vadavanath Prabhakaran V, Kozhiparambil Gopalan R. Phloretin alleviates arsenic trioxide-induced apoptosis of H9c2 cardiomyoblasts via downregulation in Ca²⁺/calcineurin/NFATc pathway and inflammatory cytokine release. *Cardiovasc Toxicol*. 2021;21:642–654. <https://doi.org/10.1007/s12012-021-09655-0>.
70. Friesner RA, Banks JL, Murphy RB, et al. Glide: A new approach for rapid, accurate docking and scoring. 1. Method and assessment of docking accuracy. *J Med Chem*. 2004;47:1739–1749. <https://doi.org/10.1021/jm0306430>.
71. Friesner RA, Murphy RB, Repasky MP, et al. Extra precision glide: Docking and scoring incorporating a model of hydrophobic enclosure for protein-ligand complexes. *J Med Chem*. 2006;49:6177–6196. <https://doi.org/10.1021/jm051256o>.
72. Sipos L, von Heijne G. Predicting the topology of eukaryotic membrane proteins. *Eur J Biochem*. 1993;213:1333–1340. <https://doi.org/10.1111/j.1432-1033.1993.tb17885.x>.
73. von Heijne G. Membrane-protein topology. *Nat Rev Mol Cell Biol*. 2006;7:909–918. <https://doi.org/10.1038/nrm2063>.
74. Baker JA, Wong WC, Eisenhaber B, Warwicker J, Eisenhaber F. Erratum to: Charged residues next to transmembrane regions revisited: “positive-inside rule” is complemented by the “negative inside depletion/outside enrichment rule”. *BMC Biol*. 2017;15:72. <https://doi.org/10.1186/s12915-017-0410-6>.
75. Maresova L, Sychrova H. Physiological characterization of *Saccharomyces cerevisiae kha1* deletion mutants. *Mol Microbiol*. 2005;55:588–600. <https://doi.org/10.1111/j.1365-2958.2004.04410.x>.
76. Horak J, Wolf DH. Glucose-induced monoubiquitination of the *Saccharomyces cerevisiae* galactose transporter is sufficient to signal its internalization. *J Bacteriol*. 2001;183:3083–3088. <https://doi.org/10.1128/JB.183.10.3083-3088.2001>.
77. Ashkenazy H, Abadi S, Martz E, et al. ConSurf 2016: An improved methodology to estimate and visualize evolutionary conservation in macromolecules. *Nucleic Acids Res*. 2016;44:W344–W350. <https://doi.org/10.1093/nar/gkw408>.
78. Sastry GM, Adzhigirey M, Day T, Annabhimoju R, Sherman W. Protein and ligand preparation: Parameters, protocols, and influence on virtual screening enrichments. *J Comput Aided Mol Des*. 2013;27:221–234. <https://doi.org/10.1007/s10822-013-9644-8>.
79. Olsson MH, Sondergaard CR, Rostkowski M, Jensen JH. Propka3: Consistent treatment of internal and surface residues in empirical pKa predictions. *J Chem Theory Comput*. 2011;7:525–537. <https://doi.org/10.1021/ct100578z>.

SUPPORTING INFORMATION

Additional supporting information can be found online in the Supporting Information section at the end of this article.

How to cite this article: Velázquez D, Průša V, Masrati G, Yariv E, Sychrova H, Ben-Tal N, et al. Allosteric links between the hydrophilic N-terminus and transmembrane core of human Na⁺/H⁺ antiporter NHA2. *Protein Science*. 2022; 31(12):e4460. <https://doi.org/10.1002/pro.4460>